https://doi.org/10.5194/egusphere-2023-2101
Preprint. Discussion started: 16 October 2023

Does dynamically modelled leaf area improve predictions of land surface water and carbon fluxes? - Insights into dynamic vegetation modules

Sven A. Westermann[1], Anke Hildebrandt[1,2], Souhail Bousetta[3], and Stephan Thober[1]

[1]Helmholtz Centre for Environmental Research GmbH - UFZ, Computational Hydrosystems, Leipzig, Germany
[2]Friedrich Schiller University Jena, Institute for Geosciences, Jena, Germany
[3]European Centre for Medium-Range Weather Forecasts, Reading, UK

Correspondence: Sven Westermann (sven.westermann@ufz.de)

Abstract. Land-surface models represent exchange processes between soil and atmosphere via the surface by coupling water, energy and carbon fluxes. As it strongly mediates the link between these cycles and, vegetation is an important component of land-surface models. In doing so, some of these models include modules for vegetation dynamics which allow adaptation of vegetation biomass, especially leaf area index, to environmental conditions. Here, we conducted a model-data comparison to investigate whether and how vegetation dynamics in the models improves the representation of vegetation processes and related surface fluxes in two specific models ECLand and Noah-MP in contrast to using prescribed values from look-up tables or satellite-based products. We compare model results with stations from the FLUXNET 2015 dataset covering a range in climate and vegetation types, the MODIS leaf area product, and use more detailed information from the TERENO site “Hohes Holz". With the current implementation, switching vegetation dynamics on did not enhance representativeness of e.g. leaf area index and net ecosystem exchange in ECLand, while Noah-MP improved it only for some sites. The representation of energy fluxes and soil moisture was almost unaffected for both models. Interestingly, for both models, the performance regarding vegetation- and hydrology-related variables was unrelated, such that the weak performance regarding e.g. leaf area index did not detoriate the performance regarding e.g. latent heat flux. One reason, we showed here, might be that implemented ecosystem processes diverge from the observations in their seasonal patterns and variability. Noah-MP includes a seasonal hysteresis of the relationship between leaf area index and gross primary production that cannot be found in observations. The same relationship is represented by a strong linear response in ECLand which substantially underestimates the variability seen in observations. For both, water and carbon fluxes, the current implemented modules for vegetation dynamics in these two models yielded no better model performance compared to runs with static vegetation and prescribed leaf-area climatology.

https://doi.org/10.5194/egusphere-2023-2101
Preprint. Discussion started: 16 October 2023

1 Introduction

Land-surface models (LSMs) represent the energy, water and biogeochemical cycles at the land surface. The main purpose has been to provide a surface component in coupled atmosphere-land models, but their scope is widening and new fields of application like historical land cover change simulations (Lawrence et al., 2018) or flood alert services (Harrigan et al., 2020) are arising. Active development within the land-surface modelling community is ongoing, adding more and more features to existing models (Blyth et al., 2021).

Given the wide use of these models and the implications of their results as they are used in the Coupled Model Intercomparison Project (CMIP), extensive model validation has been done already. Model validation covers a wide range of water, energy and carbon fluxes at global and point scale (a.o. Niu et al., 2011; Haverd et al., 2018; Lawrence et al., 2019; Boussetta et al., 2021). Such works that introduce individual evaluation schemes are accompanied by studies that perform comparisons between them like Best et al. (2015) or Krinner et al. (2018). Comparisons like those are conducted for different reasons. For example, one aim is to create a ranking between models that allows the assessment against alternative schemes. Using this method, Best et al. (2015) reported that simple statistical methods achieve a higher performance in energy partitioning at eddy-covariance sites than an ensemble of LSMs. One limitation of that study is that they did not report metrics of individual model performance, but normalized ones. This does not allow to judge whether the investigated methods achieved a (dis-)satisfactory performance. Other challenges in these activities are to maintain a standard protocol for model comparison, while not creating a superficial performance contest among them, and to minimize human errors (Menard et al., 2021).

Haughton et al. (2016) had a closer look on the cause of poor model performance of LSMs shown in the PLUMBER study by Best et al. (2015), which they presented as the bias for the evaporative fraction (EF) across various tower sites exemplarily. From all different investigated aspects they concluded that mismatches between modelled and observed heat fluxes are most likely caused by calculations within the models and not related to observations. Yet, the reasons for this mismatch, for example over-parameterization, missing processes, calibration issues etc., cannot be identified by benchmarking studies, but requires further investigation. At the same time, the causes of poor model performance can be multifaceted, rendering their identification challenging (Haughton et al., 2018b). Nonetheless, there is no way around further understanding how individual process implementation and parameterization affect model performances, if LSMs are expected to be further evolved.

A wealth of studies evaluated different LSMs with respect to radiation, heat fluxes or surface temperature, and carbon fluxes. Carbon fluxes like gross primary production (GPP), thereby, are often validated by using global gridded fluxes like FLUXNET Multi-Tree Ensembles (Ma et al., 2017; Jung et al., 2019; Lawrence et al., 2019). The correct implementation of ecosystem processes and related variables is crucial to make use of LSMs in an assessment of impacts due to climate change for example in drought evaluation (Ukkola et al., 2016; Dirmeyer et al., 2021) because plant transpiration directly links the terrestrial carbon and water cycle. Over the past decades, vegetation dynamics became more strongly determined by soil moisture (Li et al., 2022) and the sensitivity of heat flux partitioning to vegetation enlarged in turn (Forzieri et al., 2020), in particular in water-limited regions. At the same time, Li et al. (2022) reported that LSMs do misrepresent water-sensitive regions. Especially during drought events, predictions by LSMs appear to deviate from the observations. For example, a substantial underestimation of

https://doi.org/10.5194/egusphere-2023-2101
Preprint. Discussion started: 16 October 2023

evapotranspiration (ET) by eight LSMs during drought conditions was shown across different plant communities (Ukkola et al., 2016). De Kauwe et al. (2015) concluded from their simulations of drought responses for the European FLUXNET sites with the Community Atmosphere Biosphere Land Exchange (CABLE) model that accounting for differing drought sensitivity of plant communities into LSMs may be required to correctly capture drought impacts. Currently, most LSMs are not able to represent a direct vegetation control on surface exchange, amongst others because biophysical responses to changing water availability are underrepresented and vegetation, more specifically leaf area index (LAI), dynamics are simplified (Forzieri et al., 2020). LSMs typically work with climatological LAI, e.g. seasonality read from look-up table (LUT) files or calculate LAI as prognostic variable internally. At the same time, LAI has a large impact on both water and carbon fluxes (e.g. Fisher et al., 2014), and an understanding how its parameterization impacts flux estimates by LSMs helps to shed light on the known discrepancies.

Here, we investigate model performances for water and carbon fluxes especially with focus on vegetation processes. We additionally check the reasons for model-data mismatch, by analysis of the underlying computer source code of the models (as stated by Dirmeyer et al. (2018)), that can only be executed for a limited set of models. For this scope, we chose ECLand and Noah-MP as frequently used LSMs with available vegetation dynamics modules. In this manuscript, we aim to answer the following research questions: (1) Does the representation of net ecosystem exchange (NEE) and leaf area index (LAI) improve, if LSMs represent vegetation dynamically? (2) How does dynamic vegetation in those LSMs impact other variables like heat fluxes and soil moisture? Does improving one variable, compromise performance in the other or improves it along with it? (3) What are the mechanics behind different patterns in vegetation dynamics and possible misrepresentations of the observations?

2 Methods

2.1 Data basis

For this study, observational data is required for two purposes: first, as model input and, second, for performance evaluation. We used readily available data products.

Site selection

The FLUXNET 2015 dataset (Pastorello et al., 2020) provides measurements from globally distributed eddy covariance sites. We selected a subset from all the available FLUXNET sites, focusing on sites with long observation periods, covering different vegetation types and a gradient in aridity within each vegetation type. The aridity index of all sites was retrieved from the closest grid cell on a global map (Trabucco and Zomer, 2018) and inverted afterwards. We excluded sites with observation periods less than 5 years because they might not represent the local climatology (Haughton et al., 2018a). For each vegetation type (or group e.g. for savannas), first, we selected the site with the longest observation record. Next, other sites with similar aridity (± 0.1 logarithmic aridity index) were dropped to avoid including more than one representative site for each combination of aridity and vegetation type. Afterwards, we repeated these steps for the remaining sites and continued until no more sites were

https://doi.org/10.5194/egusphere-2023-2101
Preprint. Discussion started: 16 October 2023

85 available for selection. For the selected sites, we double-checked data availability and quality and replaced with an alternative site if necessary. We were left with 22 sites, covering a range of aridity and vegetation types with varying observation periods, as shown in Fig. 1, and thus, we assumed them to be neither very predictable nor very unpredictable in total, as recommended by Haughton et al. (2018a). Additionally, we also used data of the eddy covariance site "Hohes Holz" (Rebmann and Pohl, 2022) which is part of the TERENO Harz/Central German Lowland Observatory (Wollschläger et al., 2016) because on-site measured LAI data was available for that site.

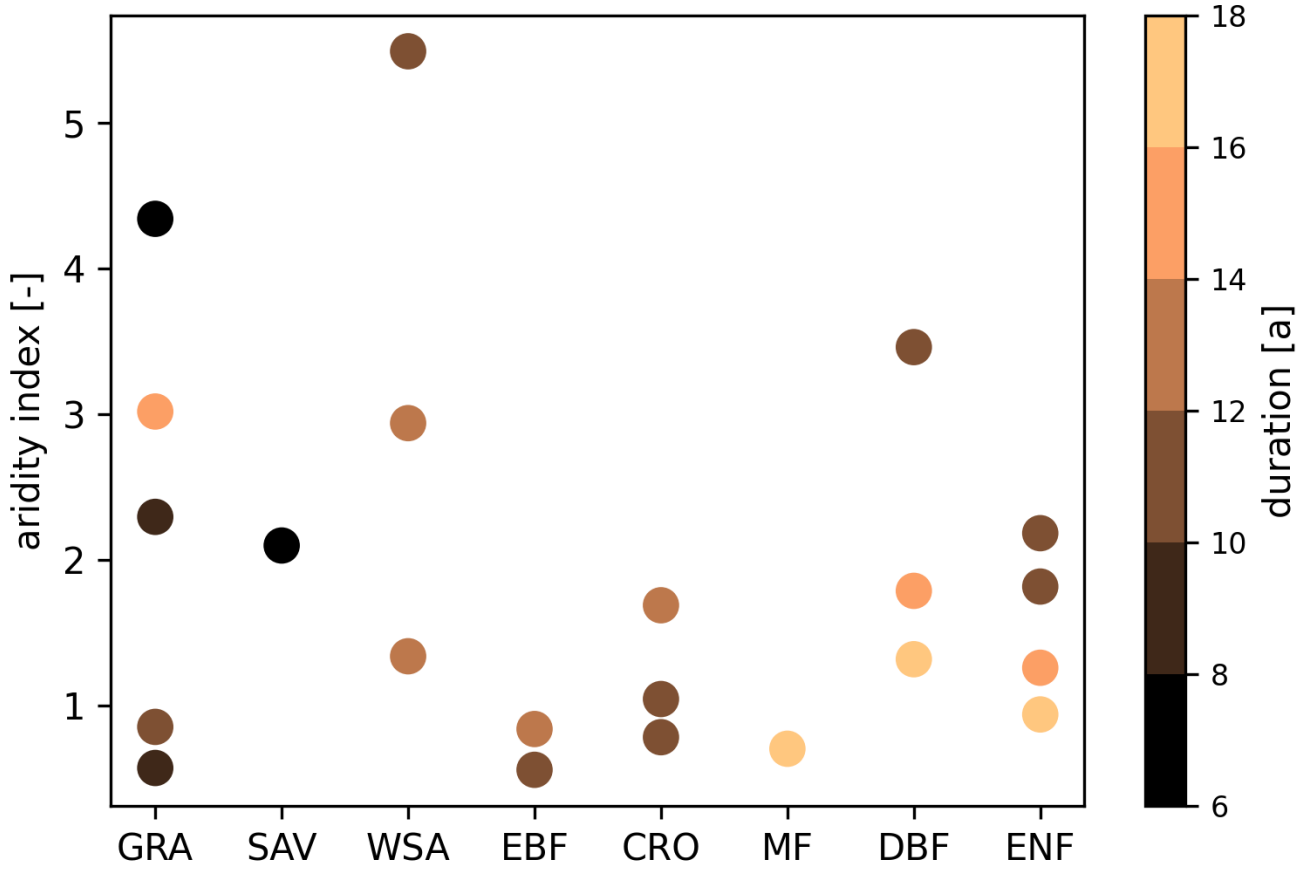

Figure 1. Selected FLUXNET sites grouped by their vegetation type. For each group, sites were chosen to cover a gradient in aridity (y-axis) if available. The vegetation types are: GRA - grassland, SAV - savanna, WSA - woody savanna, EBF - evergreen broadleaf forest, CRO - cropland, MF - mixed forest, DBF - deciduous broadleaf forest, ENF - evergreen needleleaf forest.

90

https://doi.org/10.5194/egusphere-2023-2101
Preprint. Discussion started: 16 October 2023

Variables used and data pre-processing

From the FLUXNET (Pastorello et al., 2020) and Hohes Holz (Rebmann and Pohl, 2022) datasets, air temperature, downward short- and long-wave radiation, wind speed, relative humidity, air pressure and precipitation were used for model forcing. Turbulent fluxes, e.g. latent heat flux (LE) and sensible heat flux (H), as well as net ecosystem exchange (NEE), gross primary production (GPP) and volumetric soil water content in 10 cm depth were used for model evaluation. All data were provided and used at half-hourly resolution. Missing data in the Hohes Holz meteorological dataset was filled using a Kalman filter (Sayed, 2003) for short gaps up to 3 h, except for precipitation which was set to 0. For longer gaps, filling data was retrieved from the ERA5 (Hersbach et al., 2020) data product (via Climate Data Store API from Copernicus, ©2018 ECMWF).
For calculation of the evaporative fraction $\frac{LE}{LE+H}$, all time steps with $H \leq 0$ were excluded. We adopted the same procedure to the LE values to focus comparison of turbulent fluxes on periods with evaporative demand. For performance evaluation, we excluded longer gap filled periods.

Leaf area index data and scenarios

Leaf area index (LAI) values were taken from the MOD15A2H data product from NASA's EarthData portal (Myneni et al., 2015). One grid cell was selected per eddy covariance tower according to the site coordinates and LAI values were extracted. We used LAI values with respective quality flags of 0, 32, 48 and 65 (see MODIS documentation for more details) as trade-off between excluding as much bad-flagged data as possible and keeping roughly the same amount of data values for each month. Afterwards, we smoothed the remaining values by using a Savgol filter (window length: 11, polyorder: 2) from the scipy-package (Savitzky and Golay, 1964; Luo et al., 2005) and prepared a mean annual LAI cycle for all available years with monthly resolution, further name *MODIS climatology*. For an additional experiment, the monthly LAI of the first year of the simulation period was used, called *MODIS single-year* from this point on. Each following year was then forced by the monthly MODIS LAI for that specific year. In case the LAI value for a month in that year was missing, we set it to be the mean of the adjacent months. If LAI values for more than one month were not available, the LUT LAI values were used for those months. For the Hohes Holz site, also on-site measured LAI data from Digital Hemispheric Photography was available. For each measurement date, we averaged the values from the whole plot area and, afterwards, calculated monthly means over time span 2014-2019. This alternative LAI forcing will be called *on-site LAI* hereafter. The nomenclature of all LAI scenarios can be found in Table 1.

Table 1. Nomenclature of all model scenarios using LAI data sources.

Term	LAI source
default climatological LAI	global gridded initial files (ECLand) or look-up table values per vegetation type (Noah-MP)
MODIS climatological LAI	mean annual cycle of monthly LAI values derived from MODIS dataset
MODIS single-year LAI	annual cycle of distinct years of monthly LAI values derived from MODIS dataset
on-site LAI	on-site measured LAI values

https://doi.org/10.5194/egusphere-2023-2101
Preprint. Discussion started: 16 October 2023

The MODIS LAI was also applied for model evaluation. Due to the usage of single day values, we solely used data with good quality flags (0 and 32) and refrained from smoothing. Gaps were left as they were.

2.2 Model description

We investigated how dynamic vegetation affects model outputs in two land-surface models capable of representing both static and dynamic vegetation: ECLand (Balsamo et al., 2009; Dutra et al., 2010; Boussetta et al., 2021) and Noah-MP (Chen and Dudhia, 2001; Dutra et al., 2010; Niu et al., 2007, 2011).

ECLand

The European Centre for Medium-range Weather Forecasts (ECMWF) developed a Carbon-Hydrology Tiled Scheme for Surface Exchanges over Land (CHTESSEL) (Balsamo et al., 2009; Dutra et al., 2010; Boussetta et al., 2013) which reprents the land component of the Integrated Forecasting System (IFS). As part of the IFS, CHTESSEL has evolved into a more flexible system ECLand (Boussetta et al., 2021), which also allows for several modular extensions. Among these, an under-development vegetation dynamic module simulates the temporal evolution of vegetation. Therein, LAI, vegetation biomass and vegetation coverage are calculated from the daily carbon budget, instead of taking them from the climatological LAI. However, climatological values can still be used for fully static or in partly dynamic simulations.
In ECLand (IFS cycle "CY46R1"), each of the 19 vegetation types receives its own parameter (e.g. for roughness lengths, stomata resistance to water and carbon flux, root distribution) from LUTs (Boussetta et al., 2012, 2021). These vegetation types are categorized into high or low vegetation. Each grid-cell has one dominant high and one dominant low vegetation type, together forming the vegetation of a grid-cell (Balsamo et al., 2009). Surface fluxes are computed for the high and low vegetation tiles separately then merged for the whole grid-cell according to their respective cover to be used for the vertical exchange with the atmosphere. The vegetation coverage is calculated from a prescribed climatological vegetation fraction (part of input) and a vegetation type dependent density (from LUT) and corrected by current LAI (Boussetta et al., 2021). Leaf biomass growth results from carbon accumulation of atmospheric CO_2 by the available leaf area and is restricted by environmental factors such as soil moisture and nitrogen availability. With activated vegetation dynamics, LAI depends on the built up green biomass and a LUT value of specific leaf area (Boussetta et al., 2021). For static ECLand, the prescribed climatological LAI is used. LAI in ECLand determines the canopy resistance for water vapour transport and thus, the evapotranspiration as well as the interception (Boussetta et al., 2012, 2021).

Noah-MP

Noah-MP is the widely used community Noah land-surface model (Chen and Dudhia, 2001; Dutra et al., 2010) with multi-parameterization options (Niu et al., 2007, 2011). Predicted LAI in Noah-MP is calculated based on leaf carbon allocation and specific leaf-area per vegetation type (Ma et al., 2017). In contrast to ECLand, Noah-MP can either use LAI values from LUT per vegetation type or depend solely on dynamic LAI estimates, without the option to mix between the two.

https://doi.org/10.5194/egusphere-2023-2101
Preprint. Discussion started: 16 October 2023

In Noah-MP (version "HRLDAS 3.9"), parameterization (e.g. value range of stomatal resistance, number of rooted soil layers, specific leaf area) of the 27 vegetation types is taken from LUT. The vegetated sub-grid area of each grid cell is dominated by one vegetation type forming a one-layer canopy. Calculation of canopy interception and transpiration consider aerodynamic and stomatal resistances for the water vapour and carbon fluxes within the canopy and between canopy and the atmosphere (Ma et al., 2017). Thereby, stomatal resistance is controlled by photosynthesis which depends on leaf area, and is limited by light and root zone soil moisture. Assimilated carbon, afterwards, is allocated to different plant tissues (leaf, stem, wood, root) and reduced by dying and turnover processes such as drought stress and senescence representing leaf dynamics (Dickinson et al., 1998). Carbon that is allocated to leaves converts into the LAI by using specific leaf area (Ma et al., 2017). Carbon assimilation and allocation and, thus, also GPP and NEE estimation are deactivated for the static Noah-MP since a prescribed LAI is given.

2.3 Model setup and simulations

Simulations with activated modules that predict LAI time series will be *activated vegetation dynamics* or *dynamic ECLand* and *dynamic Noah-MP* hereafter. For both models, the reference height (level of the forcing input) was set to the flux tower height of the sites which depends on the vegetation type. Forcing and model calculation were done in 30 minutes resolution if available, otherwise, hourly resolution was applied. We used four layered soil representation and used the uppermost layer for evaluation of soil moisture. Every simulation started with a ten year spin-up phase by recalculating the first year.

ECLand

We used ERA5-based (Hersbach et al., 2020) global initial data for ECLand and selected the grid cells where the flux towers are located. For the simulations that use alternative LAI forcings, monthly LAI in the initial files was replaced by the scenario specific alternative values, see section 2.1. We defined the vegetation on that grid-cell to be either high or low vegetation (and not a mixture) depending on the site information. Forests and savannas were treated as high vegetation types while grasslands, crops and shrublands were allocated to low vegetation types. Meteorological forcing was taken from the FLUXNET/TERENO data sets mentioned above (section 2.1). The ECLand simulations were done with van Genuchten soil hydrologic parameters, activated sub-grid surface runoff and activated snow parameterization.

Noah-MP

Soil type for the Noah-MP was taken from the global soil grid by PLOS ONE (Staff, 2014). The soil types of the grid-cell itself and its surrounding four neighbors were averaged. Initial values for temperatures and soil moisture were taken as the FLUXNET/TERENO observations at January 1st 00:30 h in the first year of the simulation period. Vegetation types were chosen to match as closely as possible the USGS vegetation types (©2023 UCAR)[1] and the initial LAI values were set according to the defaults in the parameter file (Table 2). Vegetation cover fraction was set to 100% so that the entire grid-cell represents the vegetation type of the observation site. Green vegetation fraction was set to 1 because otherwise temperate

[1] data can be found here: https://ral.ucar.edu/solutions/products/noah-multiparameterization-land-surface-model-noah-mp-lsm

https://doi.org/10.5194/egusphere-2023-2101
Preprint. Discussion started: 16 October 2023

short vegetation did not re-grow in spring. For the simulations with alternative LAI forcing, the monthly LAI in the LUT was replaced by the scenario specific alternative values, see section 2.1. The Noah-MP simulations were done with LUT soil parameterization, Ball-Berry stomatal resistance approach and using matric potential therefor and fully implicit temperature time schemes. Other options were used as their defaults.

Table 2. Assignment of vegetation types used in Noah-MP according to USGS classification and referred initial LAI.

Fluxnet vegetation type	Noah-MP USGS	Noah-MP vegetation class	Noah-MP initial LAI
ENF	Evergreen Needleleaf Forest	14	4.0
MF	Mixed Forest	15	2.0
DBF	Deciduous Broadleaf Forest	11	0.0
EBF	Evergreen Broadleaf Forest	13	4.5
SAV	Savanna	10	0.3
WSA	Savanna	10	0.3
OSH	Mixed Shrubland	9	0.2
CRO	Mixed Dryland/Irrigated Cropland and Pasture	4	0.0
GRA	Grassland	7	0.4

2.4 Performance evaluation

We transferred model outputs and observational data from the flux towers into daily values for direct comparison. For LAI, we calculated the eight-day mean of the LAI model output, to correspond to the temporal resolution of the MODIS LAI estimates. As performance criteria we used the Pearson's correlation coefficient, the normalized standard deviation and a modified relative bias for the model-observation relationship. Pearson's correlation coefficient R describes the fit between model and observation values (Benesty et al., 2009) and is calculated from the numpy-package as

$$R_{xy} = \frac{Cov_{xy}}{\sqrt{Cov_{xx} \cdot Cov_{yy}}} \tag{1}$$

where Cov refers to the covariance of the observations x and the model predictions y. The normalized standard deviation is the ratio of the standard deviation of the model predictions and the standard deviation of the observations. It is used to describe the models' ability to reproduce the variability of the observations. The relative bias applied here was adapted to the co-domain of the variable to avoid division by zero or by values very close to zero (especially important for NEE). Therefor, the basis of the relative bias was shifted by the minimum of the observations:

$$b = \frac{\overline{y - x}}{\overline{x} - \check{x}} \tag{2}$$

https://doi.org/10.5194/egusphere-2023-2101
Preprint. Discussion started: 16 October 2023

whereby y represents the model predictions, x the observational data, $\overline{x}$ the mean and $\check{x}$ the minimum of the observed values. To compare the model performance of static and dynamic simulations, we determined the shift in relative bias as follows:

$$\Delta b = |b_{static}| - |b_{dynamic}| \tag{3}$$

Negative values mean that the relative bias of the dynamic simulation was greater than that of the static simulation and, thus, that the performance was reduced by activating vegetation dynamics. To account for the dependence of the model performance of one target variable to that of another one we used the slope of their correlation, called *elasticity* in the following. This allows an evaluation of the impact of, for example, changing LAI representation on the GPP model performance. Elasticity is calculated as ratio of the shift in one statistical measure (analogous to equation 3) for two different target variables:

$$E = \frac{\Delta m_i}{\Delta m_j} \tag{4}$$

where m is one of the statistical measures mentioned above, e.g. R, normalized standard deviation or b, while i and j denote different target variables, e.g. GPP or latent heat flux. For variables that are strongly related, like LAI and GPP, we expect elasticitiy to be positive. Two variables were considered as independent if $-0.1 \leq E \leq 0.1$ because the change in m_j then would need to be larger than one order of magnitude to cause a change in m_i.

We plotted the shifts in model performances of the target variables in Taylor diagrams. The class design for drawing the Taylor diagrams in Python was adapted from Yannick Copin[2].

3 Results and Discussion

3.1 Using LAI climatology for ECLand and Noah-MP runs is the best way to reproduce leaf area and carbon uptake

Figure 2 shows the model quality metrics for the LAI model performance in a Taylor diagram. The point of optimal model performance is indicated with a star. The model performance of the dynamic run is shown with the symbol, while the static runs can be read from the start of each arrow. The direction and length of each arrow highlights the difference in the performance metrics between static and dynamic runs. Shown are simulations started (dynamic) or run (static) with default vs. MODIS climatological LAI. The ability of the two models to reproduce observed ecosystem variables, i.e. LAI, NEE and GPP, was in line with results in the available literature. For Noah-MP, model quality metrics were in the range of other studies, although LAI and NEE in our assessment were more biased. For ECLand, we could not find any comparable study reporting the performance of daily LAI or NEE/GPP specifically, neither for dynamic nor static simulations. However, correlation coefficients were in line with values for 10 day averages of NEE and GPP from static ECLand for a bunch of FLUXNET sites analyzed by Boussetta et al. (2013) and, by looking at mean annual cycles, Stevens et al. (2020) found a lower prediction error (RMSD) when using MODIS LAI forcing compared to LUT LAI, and, like in our study, a substantial bias.

While in simulations with static vegetation in Noah-MP the model performance depended on the applied LAI forcing, simulation results were unaffected by the type of LAI forcing with vegetation dynamics switched on (Fig. 2 c+d). This was also

[2]https://gist.github.com/ycopin/3342888, 2023-02-14

https://doi.org/10.5194/egusphere-2023-2101
Preprint. Discussion started: 16 October 2023

the case for ECLand, as for the TERENO site "Hohes Holz", but not necessarily for all sites (Fig. 2 a+b). Initializing ECLand with default climatological LAI forcing (Fig. 2 a) and activating vegetation dynamics generally increased the variance of simulated LAI but it also decreased model performance, e.g., mean Pearson correlation decreased from 0.72 to 0.62. At the same time, whether the predicted LAI fit better to MODIS observations than default climatological LAI was random, as can be seen by the shift in relative bias which ranged between -0.5 and 1.9. On the contrary, the results for Noah-MP showed a different pattern (Fig. 2 c), because there was no clear shift to higher variances or worse correlation when activating vegetation dynamics. Especially short or sparse vegetation types had the highest changes towards decreased but also enhanced model performance for LAI. For other sites (mostly forests), modelled dynamic LAI correlated well with the observations. For both models, using MODIS-based forcings in static simulations resulted in the best performances with regard to LAI of all simulations (Fig. 2 b+d), e.g., the mean correlation coefficient increased to 0.83 and 0.84 and mean relative bias improved to -16% and -2% for ECLand and Noah-MP, respectively. This can be expected because MODIS was also used as reference dataset for LAI evaluation. With activated vegetation dynamics, the performance of both models decreased, as all quality metrics shift away from the point indicating best performance in the Taylor diagram. The same applied to the relative biases of LAI since their shift was predominantly negative. In other words, switching on vegetation dynamics did not contribute to improve LAI representation compared to just using MODIS climatology. Forest ecosystems, in general, were better represented by model predictions with vegetation dynamics than short or sparse vegetation. Figure 3 shows in more detail the results of the forest site "Hohes Holz". Although the representation of LAI variability detoriated when simulating dynamic vegetation with Noah-MP, those runs resulted in LAI predictions that closely match MODIS observations (Fig. 3 d-f), represented by the relative bias of -16%. ECLand more generally suffered from large relative biases in LAI, especially when simulating with vegetation dynamics (Fig. 3 c).

Activating vegetation dynamics decreased the model performance regarding LAI for both models, especially for short and sparse vegetation types. For static ECLand, changing LAI input to MODIS climatology instead of default LAI values improved LAI representations which is expected. The default climatological LAI in ECLand is already based on MODIS data (Boussetta et al., 2012). Differing model performance regarding LAI between static runs of ECLand with default and MODIS climatological LAI, thus, has two reasons: First, the default climatological LAI was created by the disaggregating the total LAI in the MODIS data to the low and high vegetation type on the grid cell. Second, these LAI values for high and low vegetation are gridded with $10\ km$ x $10\ km$ resolution and for the MODIS climatological LAI, here, we used data from the $500\ m$ x $500\ m$ grid cell in the MODIS dataset which was closest to the flux tower. As a result, a comparison of the performance of static ECLand with either using default or MODIS climatological LAI rather shows how representative the LAI climatology is for the vegetation on that grid cell. However, in this study, adding more detailed information by using MODIS single-year LAI forcing did not further improve model performance (not shown). Updating the LAI forcing on annual time scale is far from being a near real-time data assimilation which has been shown to improve the model performance of turbulent fluxes, GPP and soil moisture for roughly 50% of the chosen sites (Boussetta et al., 2015).

For Noah-MP, static simulations with MODIS climatology had the best performance regarding LAI. However, default LAI approach was performing equally well for some sites. Substantial biases occurred for simulations with and without vegetation

https://doi.org/10.5194/egusphere-2023-2101
Preprint. Discussion started: 16 October 2023

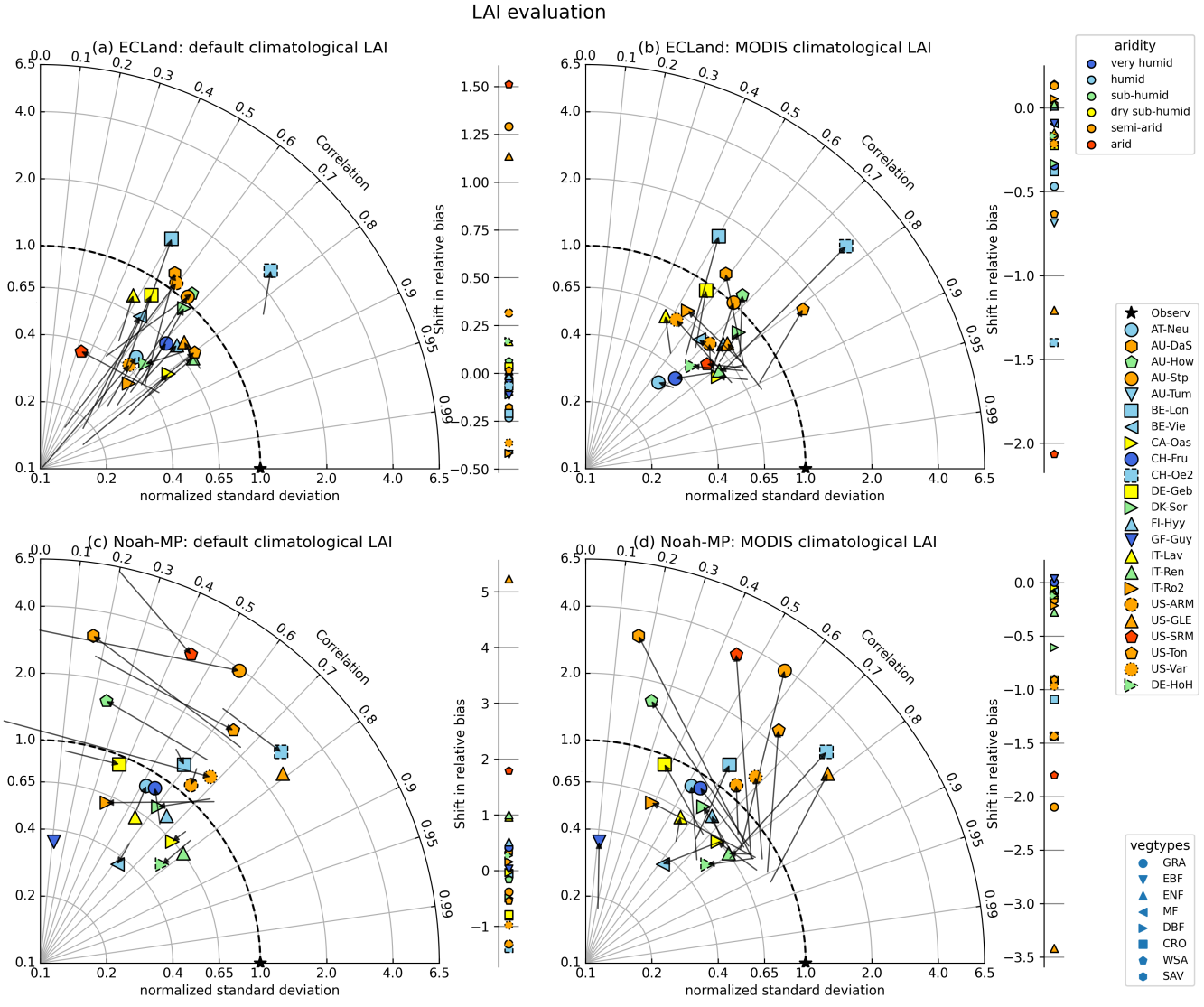

Figure 2. Change of model quality metrics for LAI modeling when switching on vegetation dynamics for all included sites and by using default climatological LAI forcing (left) or MODIS climatological LAI (right). The star ("Observ") marks the location of the perfect correlation between observation and model and perfect agreement between observed and modelled variance. The model performance of the static runs can be read from the start of each arrow. When no arrow appears, either no correlation could be calculated (e.g. for evergreen forests where default climatological LAI is constant) or values could not be placed on the logarithmic axis. The point colors indicate the site aridity (top right legend). Vegetation types are symbolized by different marker types (bottom right legend).

dynamics especially for short or sparse vegetation types, which could be due to LAI overestimation in the early growing season as reported by Cai et al. (2014). Also, Liu et al. (2016) found that neither look-up table LAI nor predicted dynamic LAI annual

https://doi.org/10.5194/egusphere-2023-2101
Preprint. Discussion started: 16 October 2023

cycles seemed to reproduce LAI observations for short vegetation. On the other hand, Pilotto et al. (2015) achieved satisfactory model predictions also for crop sites without vegetation dynamics. For short vegetation such as grasslands, the Noah-MP Crop module probably better represents LAI dynamics but we did not use this option here.

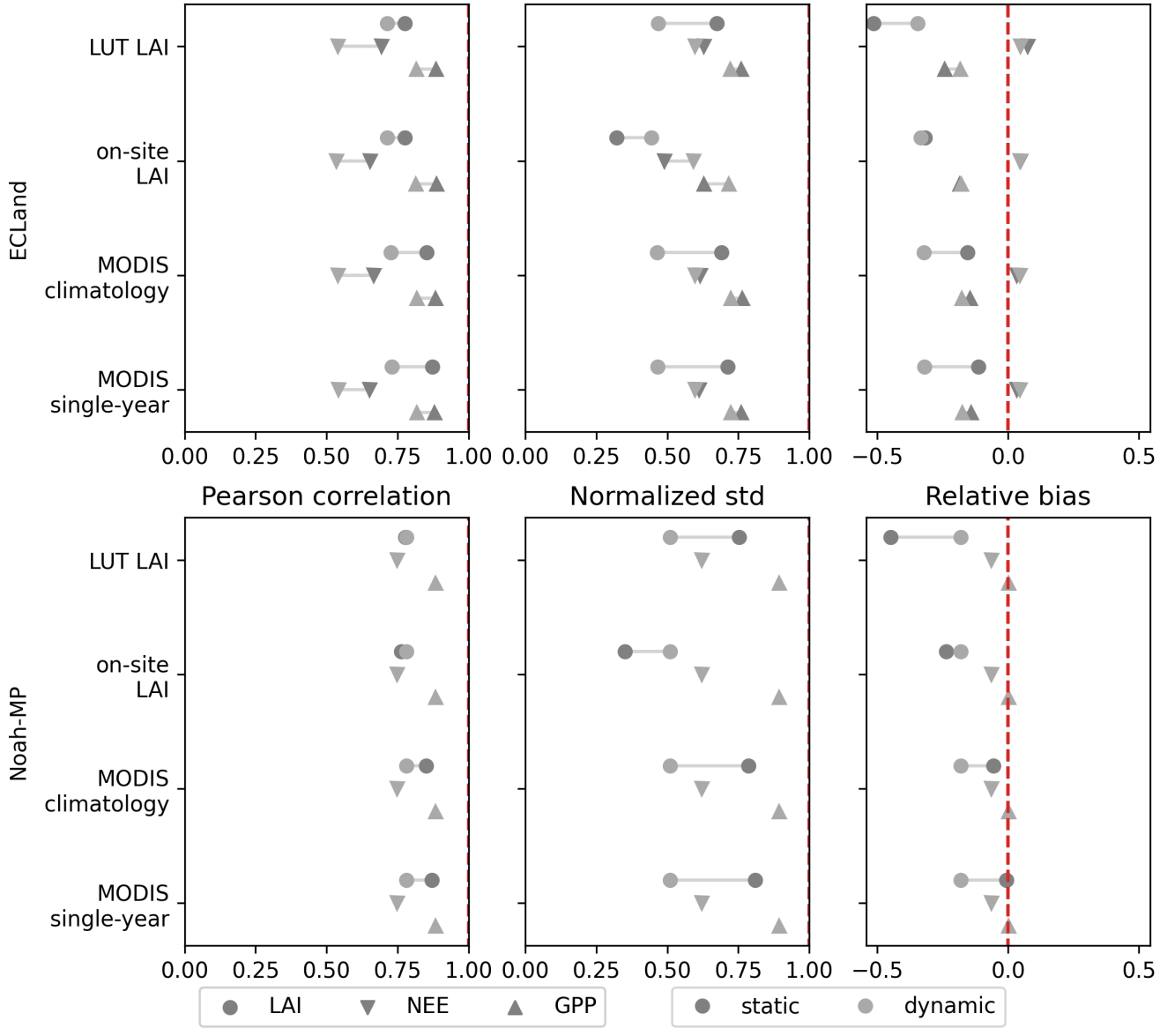

Figure 3. Statistical measures for die variables LAI, NEE and GPP of the model runs for Hohes Holz. The categories on the y-axis mark the different LAI forcings. Statistical measure of the static and dynamic simulations of the same variable are connected by a horizontal line. The red dotted vertical line marks the optimum of each measure.

https://doi.org/10.5194/egusphere-2023-2101
Preprint. Discussion started: 16 October 2023

In contrast to LAI, the model performance of ecosystem exchange variables in ECLand was less affected by activating vegetation dynamics. A common feature is, however, that the variance increased when using dynamic vegetation (Fig. 4 a+b). Mostly, sites with short or sparse vegetation reacted more sensitively to dynamic vegetation modeling in their NEE and GPP representation especially when forcing with MODIS climatology, which is indicated by the longer arrows in Fig. 4 a and b (for GPP see Fig. A1 in Appendix). For forest ecosystems in general, the changes in the model performance of NEE and GPP were small, as also shown for the TERENO site "Hohes Holz" (Fig. 3 a-c). Nevertheless, the performance of NEE and GPP decreased when activating vegetation dynamics, mainly driven by lowered correlation coefficients. Only three sites showed improvements in NEE representation when predicting with dynamic ECLand and just one did so for GPP. Dynamic ECLand mainly overestimated NEE by 11% on average, indicating that ecosystems were predicted to be a smaller carbon sink than observed. Instead, dynamic Noah-MP estimated on average 10% lower NEE compared to the observations for the most sites (Fig. 4, Fig. 3 c+f). Overall, Noah-MP seemed to capture NEE representations better as the values scattered more closely to a normalized standard deviation of 1 in the Taylor diagram and showed with 0.51 a higher correlation coefficient on average than ECLand (Fig. 4 c). Remarkably, the seven best sites regarding NEE representation in both models were forests. At the same time, both tropical forests suffered from low performance in both models. GPP representation in both models was better than for NEE (Fig. A1). Considering the opposing biases in NEE indicates that the models differ in their estimates of ecosystem respiration.

Whether switching on vegetation dynamics in Noah-MP improves NEE cannot be evaluated because it is only calculated for dynamic but not for static simulations there (see also section 2.2). Overall, dynamic Noah-MP performed well in representing NEE for most forest sites. Thus, although some previous studies found substantial overestimation in GPP for the continental U.S. (Ma et al., 2017), predicting NEE using dynamic Noah-MP could be useful in studies when LAI climatology cannot be used such as climate change impact studies. Nevertheless, short and sparse vegetation types suffered from low predictive efficiencies by dynamic Noah-MP which is in accordance with findings from Yang et al. (2021) for ChinaFLUX. There, none of the parameter sets they tested for simulations with dynamic Noah-MP resulted in well fitting predictions of diurnal changes in NEE for three of the four sites with short vegetation.

Consistent with model performances of dynamic Noah-MP being independent of the prescribed LAI forcing, the availability of on-site LAI data yielded no improvement in the representation of NEE or GPP. Interestingly, forcing ECLand with on-site LAI data even decreased model performances for NEE and GPP regardless of the choice in vegetation dynamics for the TERENO site "Hohes Holz", where on-site LAI data was available to us (Fig. 3). An assimilation of LAI during model runs and not only as fixed forcing (as in our case) might improve LAI and NEE representation which Xu et al. (2021) showed in their investigation with dynamic Noah-MP. Though, Kumar et al. (2019) could only achieve marginal improvements in GPP representation by dynamic Noah-MP due to LAI assimilation which supports our detected limited effect of LAI on simulated NEE. Similarly, the performance of NEE and GPP in ECLand was not very sensitive to different vegetation dynamics. Short or sparse vegetation types thereby were more affected by differing LAI estimates. Hence, a sensitivity analysis with respect to the impact of LAI and vegetation dynamics itself would be meaningful. In our investigation, using static ECLand simulations with MODIS climatology forcing seemed reliable in representing NEE although the correlation between modelled and observed

https://doi.org/10.5194/egusphere-2023-2101
Preprint. Discussion started: 16 October 2023

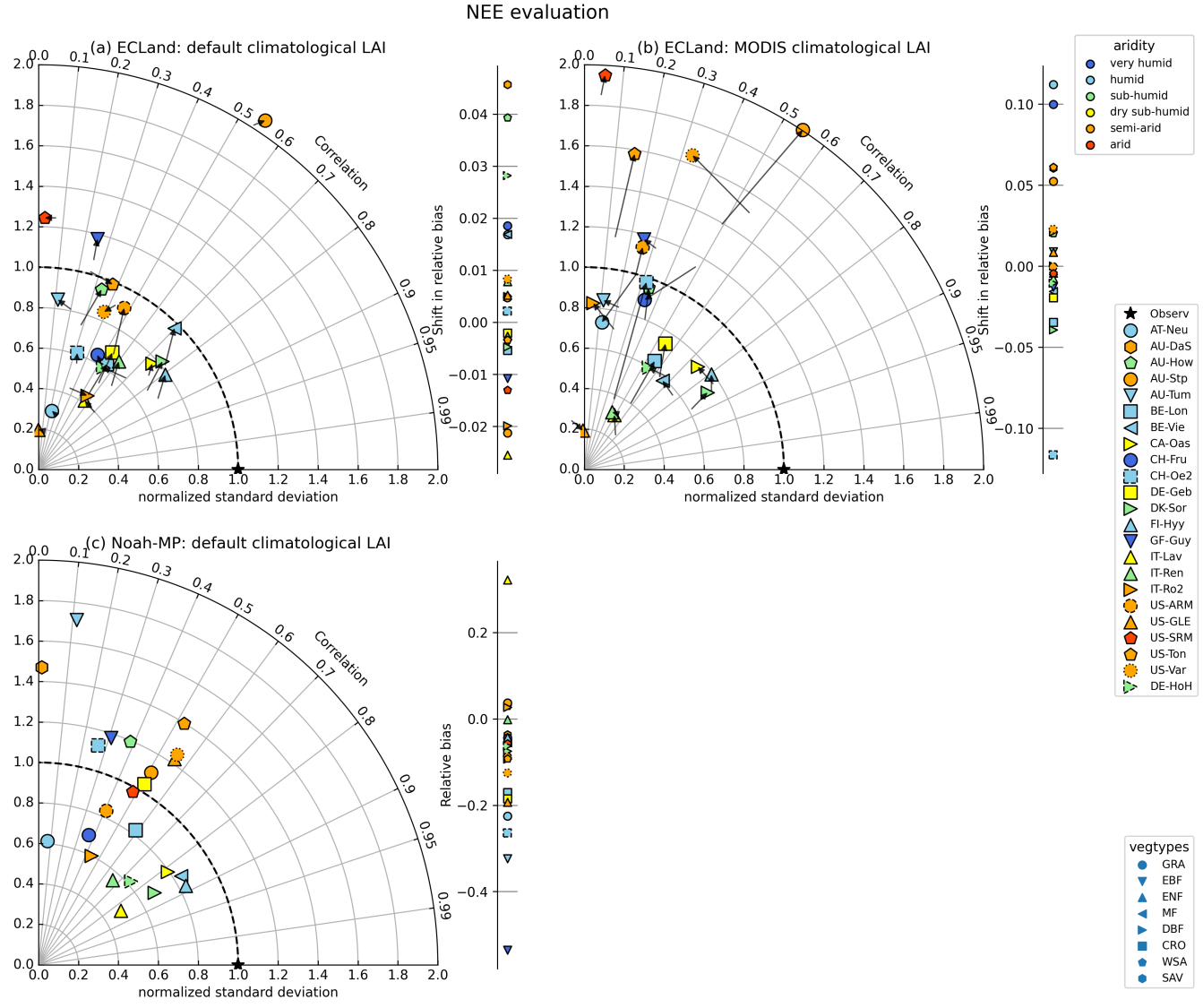

Figure 4. Same as Taylor diagram before but with NEE evaluation. Since NEE is not generated as variable from Noah-MP when running the model without dynamics, no change in statistical measures can be presented. Additionally, because all the simulations with dynamic vegetation created the same output for Noah-MP, only one Taylor diagram is shown.

300 NEE was generally low (mean Pearson correlation coefficient was 0.44). For many sites, even using the default climatological LAI for simulations with static ECLand resulted in equally good performances in simulating NEE and GPP. For modelling LAI and NEE, using dynamic vegetation modules in their current implementation in either model is not yet efficient because they increase model complexity encompassing more dynamic processes and parameters without improving fluxes predictive skill. As the dynamic vegetation components in ECLand is still under development, findings from this study will help better

https://doi.org/10.5194/egusphere-2023-2101
Preprint. Discussion started: 16 October 2023

understand and represent the processes involved to improve its performance in modeling carbon and energy fluxes. Overall, we recommend using MODIS climatology forcing or alternative remote sensing LAI products for static simulations which yields reliable model performances for NEE and GPP.

3.2 Modelled turbulent fluxes and soil moisture were almost unaffected by vegetation dynamics in both LSMs

Statistical measures for turbulent fluxes in this study were comparable to other studies. Stevens et al. (2020) found correlation coefficients of 0.79 and 0.77 for latent and sensible heat, respectively, when evaluating static ECLand simulations of the mean annual cycle with data from 17 FLUXNET stations, and Boussetta et al. (2013) showed a mean correlation coefficient of 0.81 for 10 day averages of latent heat for 32 FLUXNET sites modelled with static ECLand. We found no other studies looking explicitly at daily values for ECLand. For Noah-MP, statistical measures for turbulent fluxes and soil moisture were mostly in line with other studies (Niu et al., 2011; Yang et al., 2021; Xu et al., 2021). We found no pronounced underestimations of latent heat fluxes for humid sites as Liang et al. (2020) did in their application of Noah-MP using static vegetation representation over China.

For both models, activating vegetation dynamics had a negligible impact on the representation of turbulent fluxes and soil moisture. The strongest changes occurred for short or sparse vegetation types or for drier climates as these points appeared to have the largest arrows in the Taylor diagrams (Fig. 5, Fig. 6). In ECLand, activating vegetation dynamics enhanced the variance of latent heat flux for the most sites, but correlation between simulated and observed values remained unaffected or even diminished. For several sites, latent heat estimates from dynamic ECLand better represented the observations as shown by the positive shift in relative bias (Fig. 5 a), but no trend regarding vegetation type or site aridity can be seen and changes are small in general. Activating vegetation dynamics in Noah-MP hardly affected model performance of latent heat flux. Only sites with short or sparse vegetation types showed some sensitivity (e.g AU-Stp, US-Var, see Fig. 5 c). Several sites showed slightly enhanced fit of latent heat predictions to the observations due to vegetation dynamics in Noah-MP as can be seen by the positive shift in relative bias. When using MODIS climatology as LAI forcing, activating vegetation dynamics could be advantageous for some sites regarding latent heat flux representation, but mostly it would not lead to higher model performance.

Model performance regarding the evaporative fraction appeared to be lower compared to latent heat flux as points are further away from the point of optimal model performance (Fig. 6). Forest ecosystems thereby showed the lowest performance which is interesting since their prediction in NEE was the best. Running ECLand with activated vegetation dynamics lowered the representation of the evaporative fraction which is demonstrated by many points in the Taylor diagram drifting away from the star indicating best performance. For Noah-MP, some sites showed an improved representation of the evaporative fraction when running the model with vegetation dynamics even when the model was initialized with MODIS climatological LAI.

Regarding soil moisture, the model performance was almost insensitive to the used vegetation dynamics option or the type of LAI forcing for both models (results not shown). However, the simulation of soil moisture resulted in a broad range of model performances starting with very well-fitting predictions (correlation coefficient > 0.9, relative bias $\approx 0\%$) up to very poor-fitting predictions (correlation coefficient < 0.2, relative bias $< -40\%$ or $> 100\%$, see Tab. A6).

The impact of simulating vegetation dynamically on ECLand turbulent fluxes was small. Model performance for latent heat

https://doi.org/10.5194/egusphere-2023-2101
Preprint. Discussion started: 16 October 2023

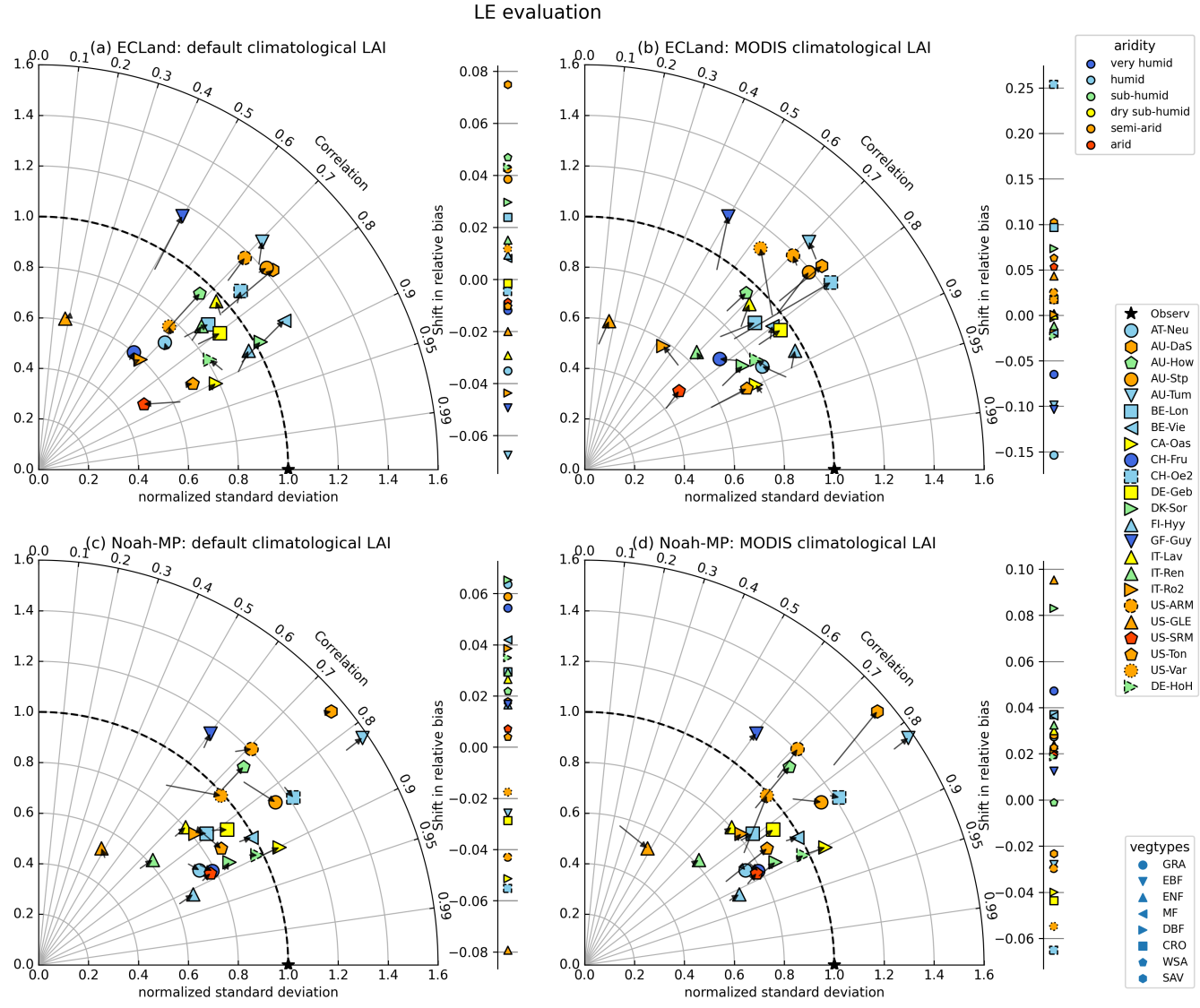

Figure 5. Change of statistical measures for latent heat modeling when switching on dynamic vegetation for all included sites and by using default climatological LAI forcing (left) or MODIS climatological LAI forcing (right).

flux and evaporative fraction changed only for some sites and towards lower performance. The predominant underestimation of latent heat flux agrees with findings of Stevens et al. (2020). For dynamic ECLand, the underestimation of GPP and LAI and might be also the reason for poor correlation of evaporative fraction between modelled and observed values. However, at the same time, Boussetta et al. (2021) found that dynamic vegetation in ECLand improved near surface temperature, sensible and turbulent heat fluxes and, hence, has the potential in improving numerical weather predictions.

Activating vegetation dynamics or changing LAI forcing had a small impact on latent heat and evaporative fraction predictions

https://doi.org/10.5194/egusphere-2023-2101
Preprint. Discussion started: 16 October 2023

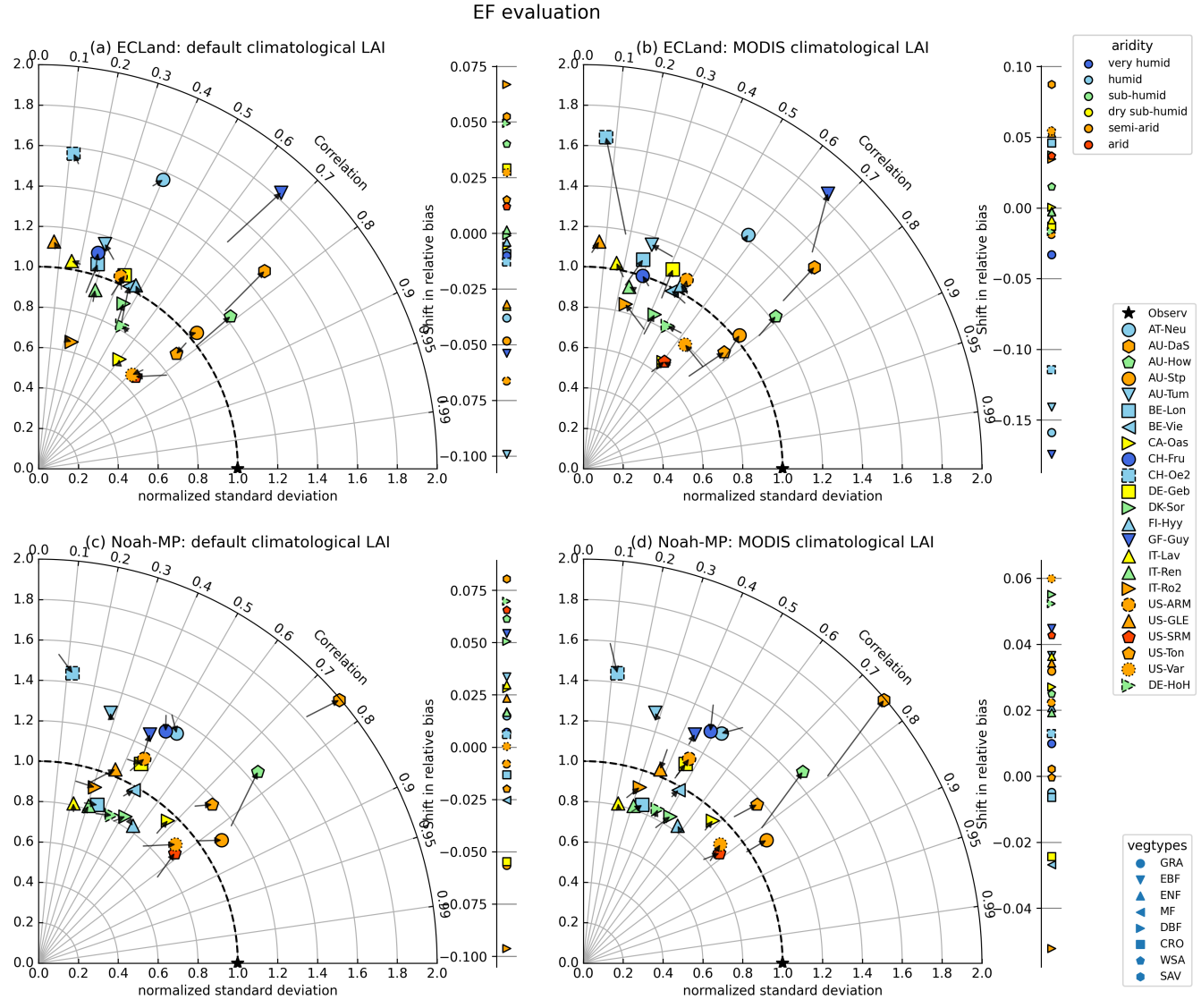

Figure 6. Same as before but for evaporative fraction which represents the turbulent flux partitioning.

with Noah-MP. Slight improvement in model performance was found for some sites with short vegetation types or semi-arid climate. Ma et al. (2017) already concluded that using LAI climatology resulted in better model performances for latent heat flux than simulations with activated vegetation dynamics for Noah-MP using the monthly FLUXNET Multi-Tree Ensemble data over the US. However, here, we did not find enhanced biases in latent heat flux predictions with dynamic Noah-MP compared to the static simulations as they did. For short vegetation types, using the Noah-MP Crop module with activated vegetation dynamics might be more sufficient in predicting surface fluxes (Liu et al., 2016).

Although vegetation and soil moisture state variables are directly coupled within land-surface models, we found almost no

https://doi.org/10.5194/egusphere-2023-2101
Preprint. Discussion started: 16 October 2023

impact of different vegetation modelling on soil moisture predictions for both models. Activating vegetation dynamics or changing LAI forcing did not improve soil moisture representation. Moreover, modelled soil moisture suffers from substantial biases in both directions which was also found by Liang et al. (2020) for Noah-MP and by Garrigues et al. (2021) for ECLand although in the latter case correlation between observed and modelled soil moisture was satisfactory (Beck et al., 2021). The reason might be underlying LUT values for soil characteristics such as field capacity and permanent wilting point that possibly deviate from on-site soil conditions and optimal values are still uncertain (Li et al., 2020). Alternatively, it could be an effect of differing scales since the observation from FLUXNET refers to point measurements. The Multiscale parameter regionalization (MPR) might provide an improved way to estimate soil parameters by applying pedo-transfer function on local soil characteristics and, recently, has been applied to Noah-MP in a proof-of-concept (Schweppe et al., 2022).

To investigate the sensitivity of dynamically modelled vegetation on the model performance, we checked how strongly the quality of the model simulation of latent heat flux and soil moisture depends on the model quality of LAI and NEE. For this, we used the elasticity (defined in section 2.4) as metric which is summarized for all sites in the bar plots of Fig. 7. Surprisingly, the model quality of those actually closely related variables was independent, i.e. the elasticity was very low (within grey band) or randomly distributed around zero. The strongest connections of all pairs tested are between NEE and latent heat flux and GPP and latent heat flux in ECLand. Here, the mean elasticity of correlation and normalized standard deviation is positive, meaning that, as expected, an increased model performance in LE co-occurs with enhanced performance for NEE and GPP, respectively. For the GPP-LE relation, even the elasticity of the relative bias is positive which underlines the co-relation of GPP and LE performances in ECLand. The fact that this is not the case for NEE might be caused by uncertainties in the predictions of respiration in the model. But elasticity values that include LAI were small predominantly. Only the correlation coefficient as model performance metric of LAI and LE in ECLand seems to be coupled but without affecting normalized standard deviation of relative bias. In other words, changes in the model quality for LAI do for most of the sites not affect the model performance of latent heat flux or soil moisture.

Notwithstanding that van den Hurk et al. (2003) at least found some effect of changed LAI values given into TESSEL, a predecessor of ECLand, as well as Ma et al. (2017) did for Noah-MP, indicating that a certain sensitivity on evapotranspiration existed. But those authors also highlighted that transpiration is only partly determined by LAI and controls through the canopy conductance for water vapour might play a larger role. However, canopy conductance is also scaled by LAI in ECland. Therefore, other compensating mechanisms may explain low elasticity between LAI and latent heat flux or soil moisture because the estimation of transpiration in the model remained almost the same as in older model versions and we also did not change any of the parameters that affect the canopy conductance. Overall, model performance regarding latent heat flux or soil moisture are independent of how LAI is represented. Thus, modelers who are mainly interested in performance of carbon processes should be careful using performance metrics for hydrological variables as a proxy (e.g. latent heat flux) because the latter might have controlling processes other than LAI or NEE which dominate the result.

In conclusion, an impact of vegetation dynamics and LAI on turbulent fluxes and soil moisture in this investigation was slim when considered across sites and seasons. However, the sensitivity to LAI might be given in some situations, since Xu et al.

https://doi.org/10.5194/egusphere-2023-2101
Preprint. Discussion started: 16 October 2023

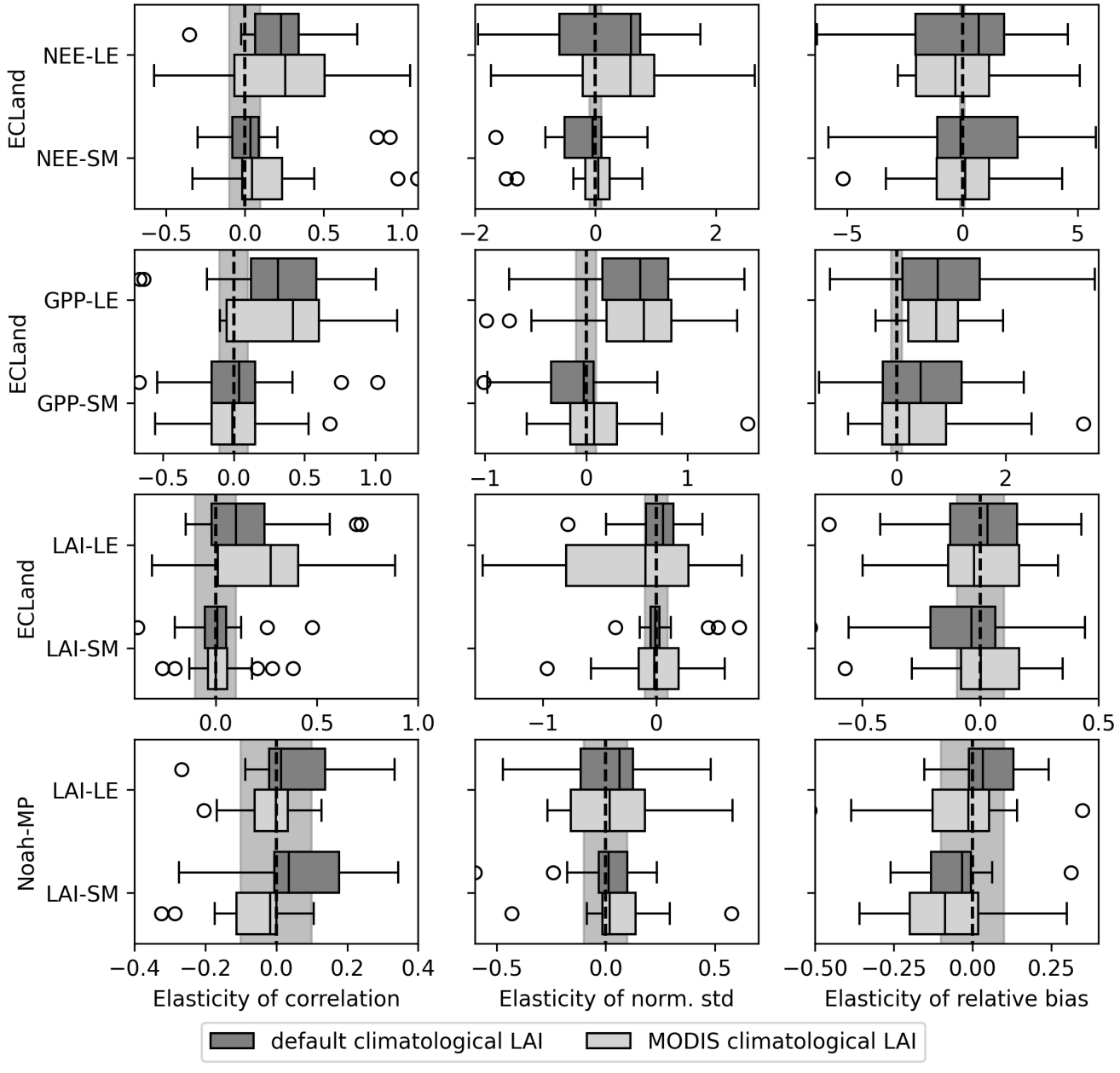

Figure 7. Box plots showing the elasticity of correlation (left column), normalized standard deviation (middle column) and relative bias (right column) for different variable relationships in both models when activating dynamic vegetation. For reasons of practicability, elasticity †is used reciprocal. Accordingly, the explanatory variable is the first one of each relationship showed on the y-axis. The grey shaded area marks the range between the thresholds of independence.

https://doi.org/10.5194/egusphere-2023-2101
Preprint. Discussion started: 16 October 2023

(2021) showed improving latent heat flux and soil moisture simulations with more realistic LAI although also there, the effect was not only site-dependent but also differed with season and year.

3.3 Observed and simulated relationships between ecohydrological variables

One possible explanation for the small contribution of model quality of LAI to that of the turbulent fluxes could be a weak relation between LAI and carbon exchange in the model. However, this is not the case as illustrated in Fig. 8. On the contrary, the relationships between GPP and LAI is much more scattered in the observations (top row) compared to the models (other rows), and this is true for both models, across biomes and vegetation types. In general, ECLand shows a linear relationship with considerable less uncertainty compared to the observations. The slope and intercept of the linear regression is dependent on the choice of static or dynamic vegetation. In contrast, Noah-MP shows a non-linear relationship with a pronounced hysteresis. This hysteresis is related to the partitioning of GPP to the carbon pools in the plants. Noah-MP uses a non-linear function for allocation of GPP to the leaves that limits the maximum LAI the model can grow.

https://doi.org/10.5194/egusphere-2023-2101
Preprint. Discussion started: 16 October 2023

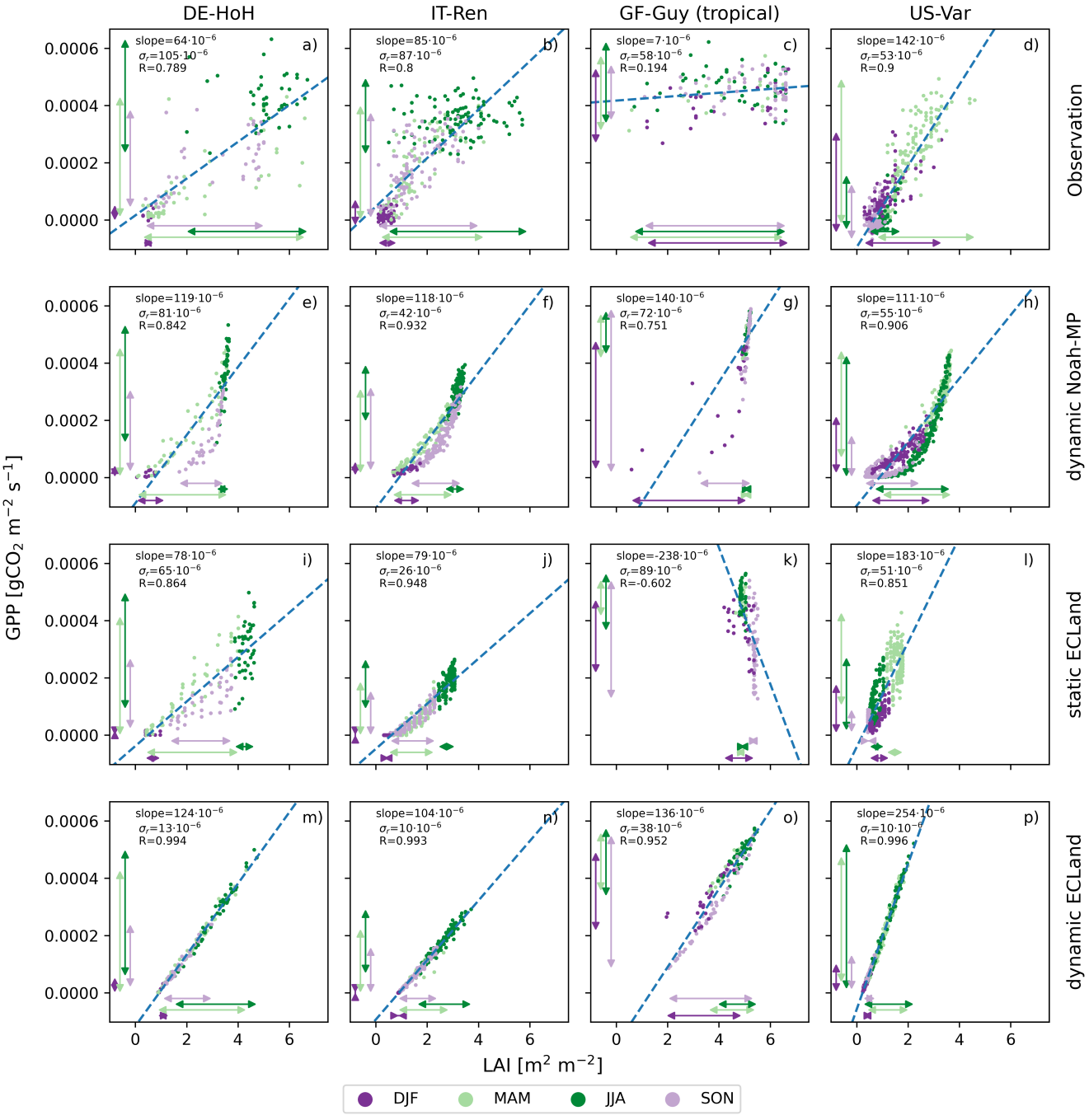

Figure 8. Scatter plots of the relationship between LAI on the x-axes and GPP on the y-axes as 8-day averages for four selected sites (columns). The rows from top to down show observations, static ECLand, dynamic ECLand, and dynamic Noah-MP. Seasons are represented by different dot colors. A simple linear regression model was applied as additional information (blue dashed line) and its correlation coefficient (R), slope and standard deviation of the residuals (σ_r) are given for each relationship.

https://doi.org/10.5194/egusphere-2023-2101
Preprint. Discussion started: 16 October 2023

Figure 8 shows the relation between GPP and LAI for four exemplary sites: DE-HoH is a deciduous broadleaf forest in a humid climate, IT-Ren is a evergreen needleleaf forest in a semi-arid climate, GF-Guy is a evergreen broadleaf forest in a tropical climate, and US-Var is a grassland in a semi-arid climate. The two European sites (left columns, De-HoH and IT-Ren) reach maximum LAI and GPP in JJA and minimum values in DJF, leading to a correlation that is mainly governed by the seasonal cycle. Similarly, at the U.S. site, with an overall tighter relation, vegetation productivity and LAI peak together in spring (i.e., MAM). For these three sites, correlation coefficients range between 0.78 to 0.90 indicating a clear but not perfect relation between LAI and GPP. However, the scatter of the observed relation is considerable with σ_r values between 53 and 105 $\cdot 10^{-6}$ $gCO_2m^{-2}s^{-1}$. The variance is highest for the peak of the growing season, when GPP quickly responds to environmental conditions (e.g., cloudiness, precipitation, and soil moisture stress) that LAI responds much slower to. The tropical site in French Guiana (GF-Guy) shows, as expected, no seasonal cycle, leading to an extremely weak relation between LAI and GPP. The latter is comparatively high all year round (GPP 0.0002 and 0.0006 $gCO_2m^{-2}s^{-1}$) although LAI values from the MODIS dataset varied between 1 and 7 m^2m^{-2}. In fact, the MODIS dataset generates some uncertainty through cloud coverage especially in the tropics. We tried to minimize this uncertainty by excluding all days from the dataset that were flagged with the value for significant cloudiness. For this tropical site, GPP and LAI dynamics seem decoupled (Fig. 8c). The substantial scatter in the observed relation between GPP and LAI is in close agreement with previous work, showing that GPP depends next to LAI also on the short-term availability of resources (e.g., light, soil water) (Hu et al., 2022). Additionally, Zhang et al. (2021) found that in LSMs the relation between LAI and GPP was too tight. We therefore checked the underlying relations in the models causing this.

Noah-MP shows a marked hysteresis effect at all sites except the tropical one (Fig. 8 e-h), with GPP linearly increasing with LAI during biomass built-up up to a point where allocation to leaves becomes minimal (vegetation type specific), and a substantial drop in GPP without any substantial reductions in LAI towards the end of the growing season (e.g., Fig. 8 e). When GPP values reduce below approximately 0.0001 $gCO_2m^{-2}s^{-1}$, then LAI reduces from values about three towards zero. A similar behaviour is observed at the grassland site in the U.S. with a shift in seasons due to local climate (Fig. 8 h). At the tropical site, Noah-MP shows some variability in GPP, but almost no change in LAI which is around a value of five.

The LAI dynamics in Noah-MP depend on a number of processes. Allocation of carbon to the leaves increases LAI, while leaf turnover and leaf die-back reduce LAI. Leaf turnover due to leaf aging is implemented as a linear function of leaf mass. Leaf die-back due to environmental limitations follows exponential functions. Taken together, leaf die-back dominates, which results in the hysteresis. The reduction of LAI (i.e., leaf die-back) is implemented to be dependent both on water and temperature stress, but temperature stress is the main driver. In the specific implementation used here, water stress only occurs at very low soil saturation of 0.1 $vol\%$ for silt loam exemplarily which is even below the permanent wilting point of this soil texture type according to the LUT value. These values are rarely reached and, thus, water stress is negligible most of the time. In contrast, temperature stress is implemented as an exponential function causing the late growing season non-linear decline of GPP observed throughout the non-tropical sites. Temperature stress is at maximum at 5 °C for forest ecosystems resulting in no active biomass below this threshold. For this reason, LAI values are almost constant at the tropical forest site because temperature is never limiting there.

https://doi.org/10.5194/egusphere-2023-2101
Preprint. Discussion started: 16 October 2023

ECLand shows a very tight linear relation between LAI and GPP with much lower scatter compared to the observations (Fig. 8 third and fourth row). ECLand with static vegetation shows similar pattern of seasonal dynamics as Noah-MP with vegetation dynamics. In contrast, dyanmic ECLand simulates LAI that is strongly coupled to daily meteorological conditions, leading to higher daily fluctuations of LAI than expected, including strong drops of LAI in summer. Three processes govern this daily LAI dynamics: GPP, respiration and senescence. GPP relates linear to LAI and varies with environmental and meteorological conditions causing the variability in static runs. In dynamic runs, losses in biomass due to high or low daily GPP linearly affect LAI. In other words, unfavourable GPP can reduce LAI almost immediately. The second process affecting LAI is senescence. ECLand distinguishes growing and senescence phase by comparing active biomass due to assimilation with biomass from previous time step. If active, then senescence is a linear function of active biomass and a folding-factor. The folding-factor reduces part of senescent biomass, depending on photosynthesis (reduced in case of high assimilation) and LAI. Overall, the folding-factor changes only slightly with LAI. Additionally, a reduction of LAI and, thus, active biomass due to reduced GPP (as explained before) causes the model to trigger senescence because the active biomass of the previous time step was higher. The third process is respiration. About 11% of physiologically possible assimilation is used for dark respiration without considering actual light conditions. This might cause high values of dark respiration compared with possible assimilation based on meteorological conditions and, thus, minimize net primary production or even produce negative values. Notably, no aboveground biomass storage is built up and there is no turnover. Most locations show a linear relationship comparable to ECLand but with a higher variability (Fig. 8 first and fourth row). This might be due to the fact that leaf growth and leaf fall, in particular for trees, happen on longer timescales than the daily one as implemented in ECLand which inhibits immediate effects of GPP on LAI.

Overall, the current implementations of leaf dynamics in both models use very different approaches to represent LAI dynamics. In Noah-MP it is mainly temperature-driven, and GPP depends little on LAI once the canopy is fully developed. In contrast, in ECLand, LAI and GPP are coupled very tightly, thus, the LAI dynamics follow almost the same sensitivities to water limitation and radiation as turbulent fluxes, which is unrealistic. However, real LAI is less dynamic and less sensitive to environmental conditions, as also indicated by the observations. Hence for very different reasons, in both models the performance regarding LAI and turbulent and carbon fluxes is disconnected.

4 Conclusions

Land-surface models often include modules for dynamic vegetation processes. However, an evaluation of the representativeness of key variables like leaf area index or net ecosystem exchange is rarely done. The impact of different parameterization of vegetation processes on water and carbon flux estimates by land-surface models is still poorly understood. Additionally, multi-model comparison studies mainly focus on internal performance rankings without deeper investigations into the reasons of performance results. Therefore, we evaluated the change in model performance of ecohydrological target variables when dynamic vegetation processes are included for two land-surface models and further gained insight into critical process implementations that lead to the observed patterns.

https://doi.org/10.5194/egusphere-2023-2101
Preprint. Discussion started: 16 October 2023

Surprisingly, neither for ECLand nor for Noah-MP, including modules for dynamic vegetation in their implementation improved the model predictions of ecohydrological variables. We expected vegetation dynamics in land-surface models to better capture the higher variability in the ecosystem exchange especially of short or sparse vegetation but this was predominantly not the case. Using alternative input for leaf area index other than default climatological values also had an negligible effect on the model performance but this needs to be evaluated in more detail. Moreover, model performances of carbon and hydrological fluxes appeared to be weakly coupled. Therefore, the question arose whether exchange fluxes themselves in these land surface models are sensitive to changes in leaf area index estimates and not only to changing parameter sets. Indeed, different leaf area index estimates lead to different predictions in exchange fluxes but without affecting the overall model performance of these variables. This might be caused by the mismatch in the seasonal patterns between observation and models for the relationship of gross primary productivity and leaf area index. While this relation in dynamic Noah-MP showed a logarithmic hysteresis, mainly driven by temperature, both variables are tightly linear coupled in dynamic ECLand without allowing for LAI to remain unchanged in suboptimal conditions for photosynthesis.

This deeper analysis of the model performance for ecohydrological fluxes that pinpoints to the reasons of model behavior was only possible with a reduced number of models. We used specific setups for the two land surface models evaluated here. Adapting or changing parameters and investigating the effect of other processes within the models were beyond the scope of this study. At this point, it remains unclear how representative our model selection is for the performance and process evaluation of other land surface models. Nonetheless, we highlighted some crucial relationships in the implementation of vegetation processes that have the potential for further improvement. Additionally, they might be a good starting point for a similar intensive investigation with other land surface models.

https://doi.org/10.5194/egusphere-2023-2101
Preprint. Discussion started: 16 October 2023

Appendix

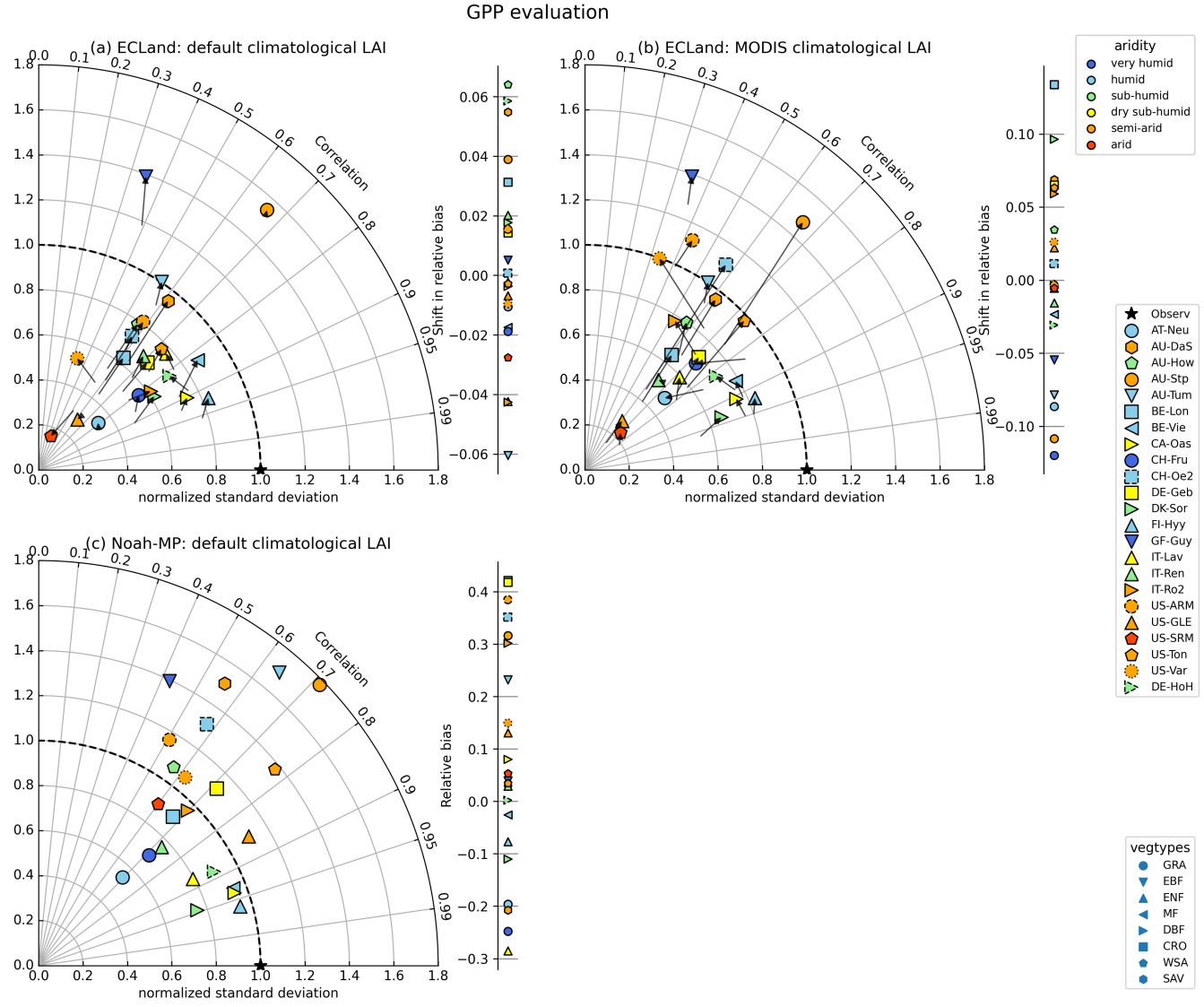

Figure A1. Change of model quality metrics for GPP prediction when switching on dynamic vegetation for all included sites and by using LUT LAI forcing (left) or MODIS LAI clomatology (right). The star ("Observ") marks the location of the perfect correlation between observation and model and perfect agreement between observed and modelled variance. The model performance of the static runs can be read from the start of each arrow. The point colors indicate the site aridity (top right legend). Vegetation types are symbolized by different marker types (bottom right legend). Since GPP is not generated as variable from Noah-MP when running the model without dynamics, no change in statistical measures can be presented. Additionally, because all the simulations with dynamic vegetation created the same output for Noah-MP, only one Taylor diagram is shown.

https://doi.org/10.5194/egusphere-2023-2101
Preprint. Discussion started: 16 October 2023

ECLand						Location	Noah-MP					
sim00	sim02	sim40	sim42	sim50	sim52		sim00	sim02	sim40	sim42	sim50	sim52
0%	0%	0%	0%	0%	0%	Obs	0%	0%	0%	0%	0%	0%
-11%	-34%	-26%	-73%	-32%	-74%	AT-Neu	-54%	-14%	6%	-14%	3%	-14%
0%	18%	-22%	20%	-36%	19%	AU-DaS	-54%	21%	-4%	21%	-1%	21%
-8%	-2%	-15%	0%	-16%	-1%	AU-How	-75%	91%	1%	91%	0%	91%
153%	-24%	-49%	-36%	-49%	-36%	AU-Stp	176%	214%	-5%	214%	-4%	214%
-31%	-74%	-3%	-72%	-2%	-72%	AU-Tum	0%	-5%	-2%	-5%	0%	-5%
27%	48%	-10%	48%	-9%	48%	BE-Lon	-28%	110%	0%	110%	1%	110%
-18%	-23%	-8%	-18%	-9%	-18%	BE-Vie	3%	9%	1%	9%	0%	9%
-4%	-13%	-12%	-11%	-13%	-11%	CA-Oas	-3%	-7%	-2%	-7%	-3%	-10%
5%	-7%	-33%	-67%	-32%	-67%	CH-Fru	-44%	-3%	-3%	-3%	-2%	-3%
127%	133%	-8%	148%	-6%	148%	CH-Oe2	6%	146%	2%	146%	4%	146%
51%	47%	-4%	26%	-6%	26%	DE-Geb	-20%	99%	8%	99%	5%	99%
-51%	-35%	-15%	-32%	-11%	-32%	DE-HoH	-45%	-18%	-6%	-18%	-1%	-18%
5%	16%	-9%	42%	-9%	42%	DK-Sor	13%	62%	1%	62%	2%	61%
-8%	-9%	-11%	-10%	-10%	-9%	FI-Hyy	62%	-11%	-1%	-11%	0%	-10%
-5%	-16%	6%	-16%	12%	-15%	GF-Guy	-7%	4%	8%	4%	7%	4%
31%	-14%	-10%	-25%	-10%	-25%	IT-Lav	109%	14%	2%	14%	2%	14%
5%	4%	-12%	-9%	-12%	-9%	IT-Ren	129%	29%	-1%	29%	-2%	29%
-4%	-46%	-13%	-7%	-13%	-8%	IT-Ro2	-38%	22%	-1%	22%	-1%	22%
32%	-1%	-36%	-53%	-37%	-53%	US-ARM	12%	144%	0%	144%	-2%	144%
263%	150%	-15%	135%	-15%	136%	US-GLE	872%	348%	-6%	348%	-5%	348%
162%	11%	-14%	221%	-14%	220%	US-SRM	365%	186%	-6%	186%	-2%	186%
29%	-28%	-14%	77%	-13%	77%	US-Ton	38%	93%	-2%	93%	0%	93%
8%	-44%	-39%	-61%	-40%	-61%	US-Var	-2%	100%	3%	100%	0%	100%

Table A1. Relative bias for LAI.

Author contributions. SW prepared model setups for the selected sites and prepared input data from available datasets in consultation with ST and AH. Model source code was provided by ST. Simulations, analysis and plotting were done by SW with the involvement of AH and ST. SW took the lead in writing the manuscript with contributions from all authors.

Competing interests. The authors declare that they have no conflict of interest.

https://doi.org/10.5194/egusphere-2023-2101
Preprint. Discussion started: 16 October 2023

ECLand						Location	Noah-MP					
sim00	sim02	sim40	sim42	sim50	sim52		sim00	sim02	sim40	sim42	sim50	sim52
0%	0%	0%	0%	0%	0%	Obs	0%	0%	0%	0%	0%	0%
-10%	-9%	-33%	-22%	-33%	-22%	AT-Neu	-	-23%	-	-23%	-	-23%
65%	61%	68%	62%	70%	62%	AU-DaS	-	-4%	-	-4%	-	-4%
64%	60%	62%	60%	62%	60%	AU-How	-	3%	-	3%	-	3%
56%	59%	65%	59%	64%	59%	AU-Stp	-	4%	-	4%	-	4%
-2%	2%	-3%	2%	-3%	2%	AU-Tum	-	-32%	-	-32%	-	-32%
-6%	-6%	-3%	-6%	-3%	-6%	BE-Lon	-	-17%	-	-17%	-	-17%
-8%	-6%	14%	16%	15%	16%	BE-Vie	-	-6%	-	-6%	-	-7%
-6%	-6%	-6%	-5%	-5%	-5%	CA-Oas	-	-9%	-	-9%	-	-10%
-4%	-2%	-14%	-4%	-14%	-4%	CH-Fru	-	-4%	-	-4%	-	-4%
-12%	-11%	-9%	-20%	-9%	-20%	CH-Oe2	-	-26%	-	-26%	-	-26%
-6%	-6%	-5%	-7%	-4%	-7%	DE-Geb	-	-18%	-	-18%	-	-18%
8%	5%	3%	5%	3%	4%	DE-HoH	-	-6%	-	-6%	-	-6%
-11%	-11%	0%	-4%	0%	-4%	DK-Sor	-	-7%	-	-7%	-	-9%
5%	6%	5%	6%	6%	6%	FI-Hyy	-	-4%	-	-4%	-	-6%
13%	14%	13%	14%	13%	14%	GF-Guy	-	-54%	-	-54%	-	-54%
44%	47%	49%	49%	49%	49%	IT-Lav	-	32%	-	32%	-	32%
3%	2%	13%	14%	13%	14%	IT-Ren	-	0%	-	0%	-	-1%
12%	14%	22%	19%	22%	19%	IT-Ro2	-	3%	-	3%	-	3%
4%	3%	-1%	-1%	-2%	-1%	US-ARM	-	-9%	-	-9%	-	-9%
-1%	-1%	1%	0%	1%	0%	US-GLE	-	-19%	-	-19%	-	-19%
28%	30%	59%	59%	59%	59%	US-SRM	-	-6%	-	-6%	-	-6%
2%	2%	15%	9%	15%	9%	US-Ton	-	-9%	-	-9%	-	-9%
-2%	-2%	-8%	-6%	-8%	-6%	US-Var	-	-13%	-	-13%	-	-13%

Table A2. Relative bias for NEE. Note that for static Noah-MP no NEE output is created.

https://doi.org/10.5194/egusphere-2023-2101
Preprint. Discussion started: 16 October 2023

ECLand						Location	Noah-MP					
sim00	sim02	sim40	sim42	sim50	sim52		sim00	sim02	sim40	sim42	sim50	sim52
0%	0%	0%	0%	0%	0%	Obs	0%	0%	0%	0%	0%	0%
-25%	-26%	-15%	-24%	-15%	-24%	AT-Neu	-	-20%	-	-20%	-	-20%
-36%	-30%	-38%	-31%	-41%	-31%	AU-DaS	-	-21%	-	-21%	-	-21%
-41%	-35%	-38%	-34%	-38%	-34%	AU-How	-	3%	-	3%	-	3%
21%	17%	5%	16%	6%	16%	AU-Stp	-	32%	-	32%	-	32%
-8%	-14%	-6%	-14%	-6%	-14%	AU-Tum	-	23%	-	23%	-	23%
-10%	-6%	-19%	-6%	-19%	-6%	BE-Lon	-	42%	-	42%	-	42%
-19%	-21%	-22%	-24%	-22%	-24%	BE-Vie	-	-3%	-	-3%	-	-3%
-14%	-15%	-13%	-14%	-14%	-14%	CA-Oas	-	8%	-	8%	-	5%
-27%	-29%	-19%	-31%	-18%	-31%	CH-Fru	-	-25%	-	-25%	-	-25%
-5%	-5%	-17%	16%	-17%	16%	CH-Oe2	-	35%	-	35%	-	35%
-5%	-4%	-12%	-5%	-13%	-5%	DE-Geb	-	42%	-	42%	-	42%
-24%	-18%	-15%	-18%	-14%	-18%	DE-HoH	-	0%	-	0%	-	0%
-36%	-34%	-37%	-27%	-37%	-27%	DK-Sor	-	11%	-	-11%	-	-11%
-25%	-25%	-25%	-25%	-25%	-25%	FI-Hyy	-	-8%	-	-8%	-	-8%
-12%	-12%	-6%	-11%	-6%	-11%	GF-Guy	-	4%	-	4%	-	4%
-45%	-49%	-58%	-58%	-59%	-58%	IT-Lav	-	-29%	-	-29%	-	-29%
-20%	-18%	-29%	-30%	-29%	-30%	IT-Ren	-	3%	-	3%	-	3%
-4%	-9%	-9%	-3%	-8%	-3%	IT-Ro2	-	30%	-	30%	-	30%
-5%	-4%	8%	8%	10%	8%	US-ARM	-	38%	-	38%	-	38%
-21%	-22%	-24%	-22%	-24%	-22%	US-GLE	-	13%	-	13%	-	13%
-17%	-20%	-22%	-23%	-22%	-23%	US-SRM	-	5%	-	5%	-	5%
-6%	-6%	-11%	-5%	-11%	-5%	US-Ton	-	3%	-	3%	-	3%
-2%	-3%	9%	6%	9%	6%	US-Var	-	15%	-	15%	-	15%

Table A3. Relative bias for GPP. Note that for static Noah-MP no GPP output is produced.

https://doi.org/10.5194/egusphere-2023-2101
Preprint. Discussion started: 16 October 2023

ECLand						Location	Noah-MP					
sim00	sim02	sim40	sim42	sim50	sim52		sim00	sim02	sim40	sim42	sim50	sim52
0%	0%	0%	0%	0%	0%	Obs	0%	0%	0%	0%	0%	0%
-36%	-40%	-13%	-28%	-13%	-28%	AT-Neu	-25%	-19%	-21%	-19%	-22%	-19%
-25%	-17%	-28%	-18%	-34%	-18%	AU-DaS	-24%	-23%	-20%	-23%	-20%	-23%
-53%	-49%	-50%	-48%	-51%	-48%	AU-How	-31%	-29%	-29%	-29%	-29%	-29%
8%	4%	3%	4%	2%	4%	AU-Stp	7%	1%	-4%	1%	-4%	1%
-11%	-17%	-7%	-17%	-7%	-17%	AU-Tum	5%	7%	4%	7%	4%	7%
-16%	-14%	-24%	-14%	-24%	-14%	BE-Lon	-3%	0%	-4%	0%	-4%	0%
8%	7%	-18%	-20%	-18%	-20%	BE-Vie	-5%	1%	-4%	1%	-4%	1%
-5%	-6%	-9%	-9%	-10%	-10%	CA-Oas	3%	8%	4%	8%	3%	7%
-36%	-37%	-24%	-31%	-24%	-31%	CH-Fru	-32%	-26%	-31%	-26%	-31%	-26%
-14%	-15%	-26%	0%	-25%	0%	CH-Oe2	3%	9%	2%	9%	2%	9%
-2%	-2%	-4%	2%	-8%	2%	DE-Geb	-2%	5%	-1%	5%	-1%	5%
-34%	-29%	-26%	-29%	-26%	-29%	DE-HoH	-17%	-14%	-16%	-14%	-15%	-14%
-7%	-4%	-37%	-29%	-37%	-29%	DK-Sor	-19%	-12%	-21%	-12%	-21%	-12%
-22%	-21%	-21%	-21%	-21%	-21%	FI-Hyy	-34%	-32%	-35%	-32%	-34%	-32%
-31%	-36%	-25%	-35%	-24%	-35%	GF-Guy	-17%	-15%	-17%	-15%	-16%	-15%
-41%	-43%	-47%	-47%	-48%	-47%	IT-Lav	-50%	-47%	-50%	-47%	-50%	-47%
-16%	-14%	-34%	-35%	-34%	-35%	IT-Ren	-37%	-35%	-38%	-35%	-38%	-34%
-12%	-17%	-39%	-39%	-39%	-39%	IT-Ro2	-9%	-6%	-8%	-6%	-8%	-6%
7%	3%	7%	4%	6%	4%	US-ARM	6%	11%	8%	11%	6%	11%
-58%	-60%	-66%	-61%	-66%	-61%	US-GLE	-52%	-59%	-69%	-59%	-69%	-59%
-21%	-21%	-27%	-21%	-26%	-22%	US-SRM	-20%	-19%	-21%	-19%	-21%	-19%
-5%	-6%	-20%	-14%	-20%	-14%	US-Ton	-10%	-10%	-12%	-10%	-12%	-10%
28%	27%	27%	26%	27%	26%	US-Var	20%	22%	16%	22%	16%	22%

Table A4. Relative bias for latent heat flux.

https://doi.org/10.5194/egusphere-2023-2101
Preprint. Discussion started: 16 October 2023

ECLand						Location	Noah-MP					
sim00	sim02	sim40	sim42	sim50	sim52		sim00	sim02	sim40	sim42	sim50	sim52
0%	0%	0%	0%	0%	0%	Obs	0%	0%	0%	0%	0%	0%
-37%	-41%	-21%	-37%	-22%	-37%	AT-Neu	-12%	-10%	-10%	-10%	-10%	-10%
-40%	-35%	-45%	-37%	-50%	-37%	AU-DaS	-51%	-43%	-43%	-43%	-43%	-43%
-49%	-45%	-46%	-45%	-47%	-45%	AU-How	-29%	-22%	-25%	-22%	-25%	-22%
-7%	-12%	-10%	-12%	-11%	-12%	AU-Stp	0%	-6%	-9%	-6%	-9%	-6%
-50%	-60%	-46%	-60%	-46%	-60%	AU-Tum	-26%	-23%	-27%	-23%	-27%	-23%
-4%	-5%	-10%	-6%	-11%	-6%	BE-Lon	8%	10%	9%	10%	9%	10%
8%	5%	-9%	-10%	-9%	-10%	BE-Vie	0%	3%	0%	3%	0%	3%
-3%	-3%	-5%	-5%	-5%	-5%	CA-Oas	-4%	-1%	-4%	-1%	-4%	-1%
-15%	-16%	-9%	-12%	-8%	-12%	CH-Fru	-9%	-8%	-9%	-8%	-9%	-8%
-43%	-45%	-18%	-29%	-18%	-29%	CH-Oe2	-4%	-4%	-5%	-4%	-5%	-4%
4%	1%	1%	3%	-2%	3%	DE-Geb	8%	13%	11%	13%	10%	13%
-56%	-51%	-49%	-51%	-48%	-51%	DE-HoH	-27%	-20%	-25%	-20%	-25%	-20%
2%	2%	-15%	-11%	-15%	-11%	DK-Sor	-9%	-4%	-10%	-4%	-10%	-4%
-5%	-6%	-5%	-6%	-6%	-6%	FI-Hyy	-11%	-10%	-12%	-10%	-12%	-10%
-73%	-78%	-60%	-78%	-59%	-77%	GF-Guy	-48%	-42%	-47%	-42%	-46%	-42%
-25%	-29%	-31%	-32%	-32%	-32%	IT-Lav	-33%	-30%	-34%	-30%	-34%	-30%
5%	5%	-6%	-6%	-6%	-6%	IT-Ren	-11%	-9%	-11%	-9%	-11%	-9%
18%	11%	-22%	-18%	-22%	-18%	IT-Ro2	6%	16%	11%	16%	11%	16%
-7%	-13%	-7%	-9%	-8%	-9%	US-ARM	1%	2%	4%	2%	3%	2%
-35%	-39%	-48%	-43%	-48%	-43%	US-GLE	-29%	-27%	-30%	-27%	-30%	-27%
-4%	-2%	-11%	-7%	-11%	-7%	US-SRM	-15%	-9%	-13%	-9%	-13%	-9%
9%	8%	-6%	0%	-6%	0%	US-Ton	1%	3%	2%	3%	2%	3%
9%	7%	6%	1%	6%	1%	US-Var	8%	8%	14%	8%	14%	8%

Table A5. Relative bias for evaporative fraction.

https://doi.org/10.5194/egusphere-2023-2101
Preprint. Discussion started: 16 October 2023

ECLand						Location	Noah-MP					
sim00	sim02	sim40	sim42	sim50	sim52		sim00	sim02	sim40	sim42	sim50	sim52
0%	0%	0%	0%	0%	0%	Obs	0%	0%	0%	0%	0%	0%
5%	6%	-5%	1%	-4%	1%	AT-Neu	-10%	-11%	-10%	-11%	-10%	-11%
687%	674%	704%	681%	709%	681%	AU-DaS	371%	353%	357%	353%	356%	353%
194%	191%	197%	193%	197%	193%	AU-How	192%	146%	169%	146%	169%	146%
102%	147%	161%	151%	160%	151%	AU-Stp	47%	41%	52%	41%	51%	41%
54%	57%	52%	57%	52%	57%	AU-Tum	29%	28%	29%	28%	29%	28%
10%	9%	14%	9%	14%	9%	BE-Lon	-8%	-13%	-8%	-13%	-8%	-13%
29%	29%	35%	36%	35%	36%	BE-Vie	7%	7%	7%	7%	7%	6%
127%	130%	132%	133%	133%	134%	CA-Oas	73%	65%	71%	65%	71%	66%
-28%	-28%	-32%	-31%	-33%	-31%	CH-Fru	-44%	-44%	-44%	-44%	-44%	-44%
50%	50%	50%	47%	50%	47%	CH-Oe2	29%	28%	29%	28%	29%	28%
97%	98%	100%	93%	102%	93%	DE-Geb	45%	27%	44%	27%	45%	27%
167%	163%	158%	163%	157%	162%	DE-HoH	111%	103%	107%	103%	107%	103%
69%	68%	79%	77%	78%	77%	DK-Sor	11%	11%	11%	11%	11%	11%
51%	50%	50%	50%	50%	50%	FI-Hyy	-3%	-4%	-3%	-4%	-4%	-5%
251%	253%	250%	253%	250%	253%	GF-Guy	160%	160%	161%	160%	160%	160%
-86%	-85%	-85%	-85%	-85%	-85%	IT-Lav	-25%	-25%	-25%	-25%	-25%	-25%
-44%	-44%	-42%	-42%	-42%	-42%	IT-Ren	-11%	-11%	-11%	-11%	-11%	-12%
-12%	-10%	13%	12%	13%	12%	IT-Ro2	-18%	-22%	-19%	-22%	-19%	-22%
17%	21%	-2%	0%	-2%	0%	US-ARM	14%	1%	16%	1%	16%	1%
48%	48%	50%	49%	50%	49%	US-GLE	36%	38%	39%	38%	39%	38%
314%	398%	552%	433%	552%	433%	US-SRM	298%	303%	339%	303%	338%	303%
7%	10%	45%	40%	45%	40%	US-Ton	6%	3%	14%	3%	14%	3%
58%	62%	72%	74%	72%	74%	US-Var	60%	53%	65%	53%	66%	53%

Table A6. Relative bias of soil moisture

https://doi.org/10.5194/egusphere-2023-2101
Preprint. Discussion started: 16 October 2023

Acknowledgements. This work used eddy covariance data acquired and shared by the FLUXNET community and by the TERENO network. On-site LAI data from site "Hohes Holz" was acquired, analyzed and shared by the working group Model Driven Monitoring lead by Corinna Rebmann at UFZ.

https://doi.org/10.5194/egusphere-2023-2101
Preprint. Discussion started: 16 October 2023

References

Balsamo, G., Viterbo, P., Beljaars, A., van den Hurk, B., Hirschi, M., Betts, A. K., and Scipal, K.: A Revised Hydrology for the ECMWF Model: Verification from Field Site to Terrestrial Water Storage and Impact in the Integrated Forecast System, Journal of Hydrometeorology, 10, 623–643, https://doi.org/10.1175/2008jhm1068.1, 2009.

Beck, H. E., Pan, M., Miralles, D. G., Reichle, R. H., Dorigo, W. A., Hahn, S., Sheffield, J., Karthikeyan, L., Balsamo, G., Parinussa, R. M., van Dijk, A. I. J. M., Du, J., Kimball, J. S., Vergopolan, N., and Wood, E. F.: Evaluation of 18 satellite- and model-based soil moisture products using in situ measurements from 826 sensors, Hydrology and Earth System Sciences, 25, 17–40, https://doi.org/10.5194/hess-25-17-2021, 2021.

Benesty, J., Chen, J., Huang, Y., and Cohen, I.: Pearson correlation coefficient, in: Noise reduction in speech processing, pp. 37–40, Springer, 2009.

Best, M. J., Abramowitz, G., Johnson, H. R., Pitman, A. J., Balsamo, G., Boone, A., Cuntz, M., Decharme, B., Dirmeyer, P. A., Dong, J., Ek, M., Guo, Z., Haverd, V., van den Hurk, B. J. J., Nearing, G. S., Pak, B., Peters-Lidard, C., Santanello, J. A., Stevens, L., and Vuichard, N.: The Plumbing of Land Surface Models: Benchmarking Model Performance, Journal of Hydrometeorology, 16, 1425–1442, https://doi.org/10.1175/jhm-d-14-0158.1, 2015.

Blyth, E. M., Arora, V. K., Clark, D. B., Dadson, S. J., De Kauwe, M. G., Lawrence, D. M., Melton, J. R., Pongratz, J., Turton, R. H., Yoshimura, K., and Yuan, H.: Advances in Land Surface Modelling, Current Climate Change Reports, 7, 45–71, https://doi.org/10.1007/s40641-021-00171-5, 2021.

Boussetta, S., Balsamo, G., Beljaars, A., Kral, T., and Jarlan, L.: Impact of a satellite-derived leaf area index monthly climatology in a global numerical weather prediction model, International Journal of Remote Sensing, 34, 3520–3542, https://doi.org/10.1080/01431161.2012.716543, 2012.

Boussetta, S., Balsamo, G., Beljaars, A., Panareda, A.-A., Calvet, J.-C., Jacobs, C., van den Hurk, B., Viterbo, P., Lafont, S., Dutra, E., Jarlan, L., Balzarolo, M., Papale, D., and van der Werf, G.: Natural land carbon dioxide exchanges in the ECMWF integrated forecasting system: Implementation and offline validation, Journal of Geophysical Research: Atmospheres, 118, 5923–5946, https://doi.org/https://doi.org/10.1002/jgrd.50488, 2013.

Boussetta, S., Balsamo, G., Dutra, E., Beljaars, A., and Albergel, C.: Assimilation of surface albedo and vegetation states from satellite observations and their impact on numerical weather prediction, Remote Sensing of Environment, 163, 111–126, https://doi.org/10.1016/j.rse.2015.03.009, 2015.

Boussetta, S., Balsamo, G., Arduini, G., Dutra, E., McNorton, J., Choulga, M., Agustí-Panareda, A., Beljaars, A., Wedi, N., Munõz-Sabater, J., de Rosnay, P., Sandu, I., Hadade, I., Carver, G., Mazzetti, C., Prudhomme, C., Yamazaki, D., and Zsoter, E.: ECLand: The ECMWF Land Surface Modelling System, Atmosphere, 12, https://doi.org/10.3390/atmos12060723, 2021.

Cai, X., Yang, Z.-L., Xia, Y., Huang, M., Wei, H., Leung, L. R., and Ek, M. B.: Assessment of simulated water balance from Noah, Noah-MP, CLM, and VIC over CONUS using the NLDAS test bed, Journal of Geophysical Research: Atmospheres, 119, 13,751–13,770, https://doi.org/10.1002/2014jd022113, 2014.

Chen, F. and Dudhia, J.: Coupling an advanced land surface-hydrology model with the Penn State-NCAR MM5 modeling system. Part I: Model implementation and sensitivity, Monthly Weather Review, 129, 569–585, https://doi.org/Doi 10.1175/1520-0493(2001)129<0569:Caalsh>2.0.Co;2, 2001.

https://doi.org/10.5194/egusphere-2023-2101
Preprint. Discussion started: 16 October 2023

De Kauwe, M. G., Zhou, S. X., Medlyn, B. E., Pitman, A. J., Wang, Y. P., Duursma, R. A., and Prentice, I. C.: Do land surface models need to include differential plant species responses to drought? Examining model predictions across a mesic-xeric gradient in Europe, Biogeosciences, 12, 7503–7518, https://doi.org/10.5194/bg-12-7503-2015, 2015.

Dickinson, R. E., Shaikh, M., Bryant, R., and Graumlich, L.: Interactive canopies for a climate model, Journal of Climate, 11, 2823–2836, https://doi.org/Doi 10.1175/1520-0442(1998)011<2823:Icfacm>2.0.Co;2, 1998.

Dirmeyer, P. A., Chen, L., Wu, J., Shin, C. S., Huang, B., Cash, B. A., Bosilovich, M. G., Mahanama, S., Koster, R. D., Santanello, J. A., Ek, M. B., Balsamo, G., Dutra, E., and Lawrence, D. M.: Verification of land-atmosphere coupling in forecast models, reanalyses and land surface models using flux site observations, J Hydrometeorol, 19, 375–392, https://doi.org/10.1175/JHM-D-17-0152.1, 2018.

Dirmeyer, P. A., Balsamo, G., Blyth, E. M., Morrison, R., and Cooper, H. M.: Land-Atmosphere Interactions Exacerbated the Drought and Heatwave Over Northern Europe During Summer 2018, AGU Advances, 2, https://doi.org/10.1029/2020av000283, 2021.

Dutra, E., Balsamo, G., Viterbo, P., Miranda, P. M. A., Beljaars, A., Schär, C., and Elder, K.: An Improved Snow Scheme for the ECMWF Land Surface Model: Description and Offline Validation, Journal of Hydrometeorology, 11, 899–916, https://doi.org/10.1175/2010jhm1249.1, 2010.

Fisher, J. B., Huntzinger, D. N., Schwalm, C. R., and Sitch, S.: Modeling the Terrestrial Biosphere, Annual Review of Environment and Resources, 39, 91–123, https://doi.org/10.1146/annurev-environ-012913-093456, 2014.

Forzieri, G., Miralles, D. G., Ciais, P., Alkama, R., Ryu, Y., Duveiller, G., Zhang, K., Robertson, E., Kautz, M., Martens, B., Jiang, C. Y., Arneth, A., Georgievski, G., Li, W., Ceccherini, G., Anthoni, P., Lawrence, P., Wiltshire, A., Pongratz, J., Piao, S. L., Sitch, S., Goll, D. S., Arora, V. K., Lienert, S., Lombardozzi, D., Kato, E., Nabel, J. E. M. S., Tian, H. Q., Friedlingstein, P., and Cescatti, A.: Increased control of vegetation on global terrestrial energy fluxes, Nature Climate Change, 10, 356–+, https://doi.org/10.1038/s41558-020-0717-0, 2020.

Garrigues, S., Verhoef, A., Blyth, E., Wright, A., Balan-Sarojini, B., Robinson, E. L., Dadson, S., Boone, A., Boussetta, S., and Balsamo, G.: Capability of the variogram to quantify the spatial patterns of surface fluxes and soil moisture simulated by land surface models, Progress in Physical Geography: Earth and Environment, 45, 279–293, https://doi.org/10.1177/0309133320986147, 2021.

Harrigan, S., Zoster, E., Cloke, H., Salamon, P., and Prudhomme, C.: Daily ensemble river discharge reforecasts and real-time forecasts from the operational Global Flood Awareness System, Hydrology and Earth System Sciences Discussions, pp. 1–22, https://doi.org/10.5194/hess-2020-532, publisher: Copernicus GmbH, 2020.

Haughton, N., Abramowitz, G., Pitman, A. J., Or, D., Best, M. J., Johnson, H. R., Balsamo, G., Boone, A., Cuntz, M., Decharme, B., Dirmeyer, P. A., Dong, J., Ek, M., Guo, Z., Haverd, V., van den Hurk, B. J. J., Nearing, G. S., Pak, B., Santanello, J. A., J., Stevens, L. E., and Vuichard, N.: The plumbing of land surface models: is poor performance a result of methodology or data quality?, J Hydrometeorol, 17, 1705–1723, https://doi.org/10.1175/JHM-D-15-0171.1, 2016.

Haughton, N., Abramowitz, G., De Kauwe, M. G., and Pitman, A. J.: Does predictability of fluxes vary between FLUXNET sites?, Biogeosciences, 15, 4495–4513, https://doi.org/10.5194/bg-15-4495-2018, 2018a.

Haughton, N., Abramowitz, G., and Pitman, A. J.: On the predictability of land surface fluxes from meteorological variables, Geoscientific Model Development, 11, 195–212, https://doi.org/10.5194/gmd-11-195-2018, 2018b.

Haverd, V., Smith, B., Nieradzik, L., Briggs, P. R., Woodgate, W., Trudinger, C. M., Canadell, J. G., and Cuntz, M.: A new version of the CABLE land surface model (Subversion revision r4601) incorporating land use and land cover change, woody vegetation demography, and a novel optimisation-based approach to plant coordination of photosynthesis, Geoscientific Model Development, 11, 2995–3026, https://doi.org/10.5194/gmd-11-2995-2018, 2018.

https://doi.org/10.5194/egusphere-2023-2101
Preprint. Discussion started: 16 October 2023

Hersbach, H., Bell, B., Berrisford, P., Hirahara, S., Horányi, A., Muñoz-Sabater, J., Nicolas, J., Peubey, C., Radu, R., Schepers, D., Simmons, A., Soci, C., Abdalla, S., Abellan, X., Balsamo, G., Bechtold, P., Biavati, G., Bidlot, J., Bonavita, M., De Chiara, G., Dahlgren, P., Dee, D., Diamantakis, M., Dragani, R., Flemming, J., Forbes, R., Fuentes, M., Geer, A., Haimberger, L., Healy, S., Hogan, R. J., Hólm, E., Janisková, M., Keeley, S., Laloyaux, P., Lopez, P., Lupu, C., Radnoti, G., de Rosnay, P., Rozum, I., Vamborg, F., Villaume, S., and Thépaut, J.-N.: The ERA5 global reanalysis, Q. J. Roy. Meteor. Soc., n/a, https://doi.org/10.1002/qj.3803, 2020.

Hu, Z., Piao, S., Knapp, A. K., Wang, X., Peng, S., Yuan, W., Running, S., Mao, J., Shi, X., Ciais, P., Huntzinger, D. N., Yang, J., and Yu, G.: Decoupling of greenness and gross primary productivity as aridity decreases, Remote Sensing of Environment, 279, 113 120, https://doi.org/10.1016/j.rse.2022.113120, 2022.

Jung, M., Koirala, S., Weber, U., Ichii, K., Gans, F., Camps-Valls, G., Papale, D., Schwalm, C., Tramontana, G., and Reichstein, M.: The FLUXCOM ensemble of global land-atmosphere energy fluxes, Scientific Data, 6, 74, https://doi.org/10.1038/s41597-019-0076-8, 2019.

Krinner, G., Derksen, C., Essery, R., Flanner, M., Hagemann, S., Clark, M., Hall, A., Rott, H., Brutel-Vuilmet, C., Kim, H., Ménard, C. B., Mudryk, L., Thackeray, C., Wang, L., Arduini, G., Balsamo, G., Bartlett, P., Boike, J., Boone, A., Chéruy, F., Colin, J., Cuntz, M., Dai, Y., Decharme, B., Derry, J., Ducharne, A., Dutra, E., Fang, X., Fierz, C., Ghattas, J., Gusev, Y., Haverd, V., Kontu, A., Lafaysse, M., Law, R., Lawrence, D., Li, W., Marke, T., Marks, D., Ménégoz, M., Nasonova, O., Nitta, T., Niwano, M., Pomeroy, J., Raleigh, M. S., Schaedler, G., Semenov, V., Smirnova, T. G., Stacke, T., Strasser, U., Svenson, S., Turkov, D., Wang, T., Wever, N., Yuan, H., Zhou, W., and Zhu, D.: ESM-SnowMIP: assessing snow models and quantifying snow-related climate feedbacks, Geoscientific Model Development, 11, 5027–5049, https://doi.org/10.5194/gmd-11-5027-2018, 2018.

Kumar, S. V., M. Mocko, D., Wang, S., Peters-Lidard, C. D., and Borak, J.: Assimilation of Remotely Sensed Leaf Area Index into the Noah-MP Land Surface Model: Impacts on Water and Carbon Fluxes and States over the Continental United States, Journal of Hydrometeorology, 20, 1359–1377, https://doi.org/10.1175/jhm-d-18-0237.1, 2019.

Lawrence, D. M., Fisher, R. A., Koven, C. D., Oleson, K. W., Swenson, S. C., Bonan, G., Collier, N., Ghimire, B., van Kampenhout, L., Kennedy, D., Kluzek, E., Lawrence, P. J., Li, F., Li, H., Lombardozzi, D., Riley, W. J., Sacks, W. J., Shi, M., Vertenstein, M., Wieder, W. R., Xu, C., Ali, A. A., Badger, A. M., Bisht, G., van den Broeke, M., Brunke, M. A., Burns, S. P., Buzan, J., Clark, M., Craig, A., Dahlin, K., Drewniak, B., Fisher, J. B., Flanner, M., Fox, A. M., Gentine, P., Hoffman, F., Keppel-Aleks, G., Knox, R., Kumar, S., Lenaerts, J., Leung, L. R., Lipscomb, W. H., Lu, Y., Pandey, A., Pelletier, J. D., Perket, J., Randerson, J. T., Ricciuto, D. M., Sanderson, B. M., Slater, A., Subin, Z. M., Tang, J., Thomas, R. Q., Val Martin, M., and Zeng, X.: The Community Land Model Version 5: Description of New Features, Benchmarking, and Impact of Forcing Uncertainty, Journal of Advances in Modeling Earth Systems, 11, 4245–4287, https://doi.org/10.1029/2018MS001583, _eprint: https://onlinelibrary.wiley.com/doi/pdf/10.1029/2018MS001583, 2019.

Lawrence, P. J., Lawrence, D. M., and Hurtt, G. C.: Attributing the Carbon Cycle Impacts of CMIP5 Historical and Future Land Use and Land Cover Change in the Community Earth System Model (CESM1), Journal of Geophysical Research: Biogeosciences, 123, 1732–1755, https://doi.org/10.1029/2017jg004348, 2018.

Li, J., Chen, F., Lu, X., Gong, W., Zhang, G., and Gan, Y.: Quantifying Contributions of Uncertainties in Physical Parameterization Schemes and Model Parameters to Overall Errors in Noah-MP Dynamic Vegetation Modeling, Journal of Advances in Modeling Earth Systems, 12, https://doi.org/10.1029/2019ms001914, 2020.

Li, W., Migliavacca, M., Forkel, M., Denissen, J. M. C., Reichstein, M., Yang, H., Duveiller, G., Weber, U., and Orth, R.: Widespread increasing vegetation sensitivity to soil moisture, Nat Commun, 13, 3959, https://doi.org/10.1038/s41467-022-31667-9, 2022.

https://doi.org/10.5194/egusphere-2023-2101
Preprint. Discussion started: 16 October 2023

Liang, J., Yang, Z.-L., Cai, X., Lin, P., Zheng, H., and Bian, Q.: Modeling the Impacts of Nitrogen Dynamics on Regional Terrestrial Carbon and Water Cycles over China with Noah-MP-CN, Advances in Atmospheric Sciences, 37, 679–695, https://doi.org/10.1007/s00376-020-9231-6, 2020.

Liu, X., Chen, F., Barlage, M., Zhou, G., and Niyogi, D.: Noah-MP-Crop: Introducing dynamic crop growth in the Noah-MP land surface model, Journal of Geophysical Research: Atmospheres, 121, 13,953–13,972, https://doi.org/10.1002/2016jd025597, 2016.

Luo, J., Ying, K., and Bai, J.: Savitzky-Golay smoothing and differentiation filter for even number data, Signal Processing, 85, 1429–1434, https://doi.org/10.1016/j.sigpro.2005.02.002, 2005.

Ma, N., Niu, G.-Y., Xia, Y., Cai, X., Zhang, Y., Ma, Y., and Fang, Y.: A Systematic Evaluation of Noah-MP in Simulating Land-Atmosphere Energy, Water, and Carbon Exchanges Over the Continental United States, Journal of Geophysical Research: Atmospheres, 122, 12,245–12,268, https://doi.org/10.1002/2017jd027597, 2017.

Menard, C. B., Essery, R., Krinner, G., Arduini, G., Bartlett, P., Boone, A., Brutel-Vuilmet, C., Burke, E., Cuntz, M., Dai, Y., Decharme, B., Dutra, E., Fang, X., Fierz, C., Gusev, Y., Hagemann, S., Haverd, V., Kim, H., Lafaysse, M., Marke, T., Nasonova, O., Nitta, T., Niwano, M., Pomeroy, J., Schädler, G., Semenov, V. A., Smirnova, T., Strasser, U., Swenson, S., Turkov, D., Wever, N., and Yuan, H.: Scientific and Human Erros in a Snow Model Intercomparison, https://doi.org/https://doi.org/10.1175/BAMS-D-19-0329.1, 2021.

Myneni, R., Knyazikhin, Y., and Park, T.: MOD15A2H MODIS/Terra Leaf Area Index/FPAR 8-Day L4 Global 500m SIN Grid V006, https://doi.org/https://doi.org/10.5067/MODIS/MOD15A2H.006, 2015.

Niu, G.-Y., Yang, Z.-L., Dickinson, R. E., Gulden, L. E., and Su, H.: Development of a simple groundwater model for use in climate models and evaluation with Gravity Recovery and Climate Experiment data, Journal of Geophysical Research, 112, https://doi.org/10.1029/2006jd007522, 2007.

Niu, G.-Y., Yang, Z.-L., Mitchell, K. E., Chen, F., Ek, M. B., Barlage, M., Kumar, A., Manning, K., Niyogi, D., Rosero, E., Tewari, M., and Xia, Y.: The community Noah land surface model with multiparameterization options (Noah-MP): 1. Model description and evaluation with local-scale measurements, Journal of Geophysical Research, 116, https://doi.org/10.1029/2010jd015139, 2011.

Pastorello, G., Trotta, C., Canfora, E., Chu, H., Christianson, D., Cheah, Y. W., Poindexter, C., Chen, J., Elbashandy, A., Humphrey, M., Isaac, P., Polidori, D., Reichstein, M., Ribeca, A., van Ingen, C., Vuichard, N., Zhang, L., Amiro, B., Ammann, C., Arain, M. A., Ardo, J., Arkebauer, T., Arndt, S. K., Arriga, N., Aubinet, M., Aurela, M., Baldocchi, D., Barr, A., Beamesderfer, E., Marchesini, L. B., Bergeron, O., Beringer, J., Bernhofer, C., Berveiller, D., Billesbach, D., Black, T. A., Blanken, P. D., Bohrer, G., Boike, J., Bolstad, P. V., Bonal, D., Bonnefond, J. M., Bowling, D. R., Bracho, R., Brodeur, J., Brummer, C., Buchmann, N., Burban, B., Burns, S. P., Buysse, P., Cale, P., Cavagna, M., Cellier, P., Chen, S., Chini, I., Christensen, T. R., Cleverly, J., Collalti, A., Consalvo, C., Cook, B. D., Cook, D., Coursolle, C., Cremonese, E., Curtis, P. S., D'Andrea, E., da Rocha, H., Dai, X., Davis, K. J., Cinti, B., Grandcourt, A., Ligne, A., De Oliveira, R. C., Delpierre, N., Desai, A. R., Di Bella, C. M., Tommasi, P. D., Dolman, H., Domingo, F., Dong, G., Dore, S., Duce, P., Dufrene, E., Dunn, A., Dusek, J., Eamus, D., Eichelmann, U., ElKhidir, H. A. M., Eugster, W., Ewenz, C. M., Ewers, B., Famulari, D., Fares, S., Feigenwinter, I., Feitz, A., Fensholt, R., Filippa, G., Fischer, M., Frank, J., Galvagno, M., Gharun, M., et al.: The FLUXNET2015 dataset and the ONEFlux processing pipeline for eddy covariance data, Sci Data, 7, 225, https://doi.org/10.1038/s41597-020-0534-3, 2020.

Pilotto, I. L., Rodríguez, D. A., Tomasella, J., Sampaio, G., and Chou, S. C.: Comparisons of the Noah-MP land surface model simulations with measurements of forest and crop sites in Amazonia, Meteorology and Atmospheric Physics, 127, 711–723, https://doi.org/10.1007/s00703-015-0399-8, 2015.

Rebmann, C. and Pohl, F.: Carbon, water and energy fluxes at the TERENO/ICOS ecosystem station Hohes Holz in Central Germany since 2015, https://doi.org/https://doi.pangaea.de/10.1594/PANGAEA.940760, 2022.

https://doi.org/10.5194/egusphere-2023-2101
Preprint. Discussion started: 16 October 2023

Savitzky, A. and Golay, M. J. E.: Smoothing + Differentiation of Data by Simplified Least Squares Procedures, Analytical Chemistry, 36, 1627–, https://doi.org/DOI 10.1021/ac60214a047, 1964.

Sayed, A. H.: Fundamentals of adaptive filtering, John Wiley & Sons, 2003.

Schweppe, R., Thober, S., Müller, S., Kelbling, M., Kumar, R., Attinger, S., and Samaniego, L.: MPR 1.0: a stand-alone multiscale parameter regionalization tool for improved parameter estimation of land surface models, Geoscientific Model Development, 15, 859–882, https://doi.org/10.5194/gmd-15-859-2022, 2022.

Staff, T. P. O.: Correction: SoilGrids1km — Global Soil Information Based on Automated Mapping, PLoS ONE, 9, https://doi.org/10.1371/journal.pone.0114788, 2014.

Stevens, D., Miranda, P. M. A., Orth, R., Boussetta, S., Balsamo, G., and Dutra, E.: Sensitivity of Surface Fluxes in the ECMWF Land Surface Model to the Remotely Sensed Leaf Area Index and Root Distribution: Evaluation with Tower Flux Data, Atmosphere, 11, https://doi.org/10.3390/atmos11121362, 2020.

Trabucco, A. and Zomer, R. J.: Global Aridity Index and Potential Evapo-Transpiration (ET0) Climate Database v2, CGIAR-CSI GeoPortal, 2018.

Ukkola, A. M., De Kauwe, M. G., Pitman, A. J., Best, M. J., Abramowitz, G., Haverd, V., Decker, M., and Haughton, N.: Land surface models systematically overestimate the intensity, duration and magnitude of seasonal-scale evaporative droughts, Environmental Research Letters, 11, https://doi.org/10.1088/1748-9326/11/10/104012, 2016.

van den Hurk, B. J. J. M., Viterbo, P., and Los, S. O.: Impact of leaf area index seasonality on the annual land surface evaporation in a global circulation model, Journal of Geophysical Research: Atmospheres, 108, https://doi.org/10.1029/2002jd002846, 2003.

Wollschläger, U., Attinger, S., Borchardt, D., Brauns, M., Cuntz, M., Dietrich, P., Fleckenstein, J. H., Friese, K., Friesen, J., Harpke, A., Hildebrandt, A., Jäckel, G., Kamjunke, N., Knöller, K., Kögler, S., Kolditz, O., Krieg, R., Kumar, R., Lausch, A., Liess, M., Marx, A., Merz, R., Mueller, C., Musolff, A., Norf, H., Oswald, S. E., Rebmann, C., Reinstorf, F., Rode, M., Rink, K., Rinke, K., Samaniego, L., Vieweg, M., Vogel, H.-J., Weitere, M., Werban, U., Zink, M., and Zacharias, S.: The Bode hydrological observatory: a platform for integrated, interdisciplinary hydro-ecological research within the TERENO Harz/Central German Lowland Observatory, Environmental Earth Sciences, 76, https://doi.org/10.1007/s12665-016-6327-5, 2016.

Xu, T., Chen, F., He, X., Barlage, M., Zhang, Z., Liu, S., and He, X.: Improve the Performance of the Noah-MP-Crop Model by Jointly Assimilating Soil Moisture and Vegetation Phenology Data, Journal of Advances in Modeling Earth Systems, 13, https://doi.org/10.1029/2020ms002394, 2021.

Yang, Q., Dan, L., Lv, M., Wu, J., Li, W., and Dong, W.: Quantitative assessment of the parameterization sensitivity of the Noah-MP land surface model with dynamic vegetation using ChinaFLUX data, Agricultural and Forest Meteorology, 307, https://doi.org/10.1016/j.agrformet.2021.108542, 2021.

Zhang, Z., Xin, Q., and Li, W.: Machine Learning-Based Modeling of Vegetation Leaf Area Index and Gross Primary Productivity Across North America and Comparison With a Process-Based Model, Journal of Advances in Modeling Earth Systems, p. 25, https://doi.org/10.1029/2021MS002802, 2021.